Real-time oxygen sensing as a powerful tool to investigate tyrosinase kinetics allows revising mechanism and activity of inhibition by glabridin

Real-time oxygen sensing as a powerful tool to investigate tyrosinase kinetics allows revising mechanism and activity of inhibition by glabridin

Yafang Guo,[a] Alice Cariola,[a] Riccardo Matera,[b] Simone Gabbanini,[b] & Luca Valgimigli*,[a]

[a] *University of Bologna, Department of Chemistry "G. Ciamician", Via S. Giacomo 1, 40126 Bologna, Italy*

[b] *BeC s.r.l., R&D Division, Via C. Monteverdi 49, 47122 Forlì, Italy*

***** to whom correspondence should be addressed. Tel. +390512095683

E-mail: luca.valgimigli@unibo.it

Y. G. yafang.guo@unibo.it; A.C. alice.cariola2@unibo.it; R.M. ricerca@bec-natura.com; S.G. laboratorio@bec-natura.com

Abstract

A new method for studying tyrosinase kinetics and inhibition by oxygen sensing is described and matched to the conventional spectrophotometric approach. The stoichiometric ratio of O_2 uptake to dopachrome formation was 1.5±0.2 for substrate L-tyrosine and 1.0±0.1 for L-DOPA. With both methods, we reinvestigated mushroom tyrosinase inhibition by glabridin from *Glycyrrhiza glabra*. The two methods agreed showing mixed-type inhibition for monophenolase and diphenolase activities, at variance with previous literature. Average K_I (K_{SI}) values for glabridin were 13.6±3.5 (281±89) nM and 57±8 (1312±550) nM, for monophenolase and diphenolase inhibition, respectively, with IC_{50} of 80±8 nM and 294±25 nM, respectively, at 1 mM substrate. For reference kojic acid K_I (K_{SI}) were 10.9±8 (217±55) μM and 9.9±1.4 (21.0±5.2) μM, for monophenolase and diphenolase, respectively, with respective IC_{50} of 33±8 μM and 17±3 μM. Glabridin's activity is among the highest in nature, being about three orders of magnitude higher than previously reported.

Keywords: glabridin, kojic acid, mushroom tyrosinase, inhibition kinetics, oximetry.

Products investigated in this study:

Mushroom Tyrosinase (EC 1.14.18.1), CAS: 9002-10-2

Glabridin, CAS: 59870-68-7 (PubChem CID: 124052)

Kojic acid, CAS: 501-30-4; (PubChem CID: 3840)

1. Introduction

Melanin is a group of organic pigments widely distributed in different kingdoms, from bacteria to fungi, to plants and animals, including humans (d'Ischia et al., 2015). It is biosynthesized from the oxidation and polymerization of phenolic precursors, mainly by the action of tyrosinase (TY) enzyme. Melanins, particularly Eumelanins, have important biological functions and properties, which are still the object of extensive research, most notably: photo-protection, protection from ionizing radiations, neuroprotection and antioxidant (d'Ischia et al., 2015; Guo et al., 2021). Their multiple properties justify the major interest melanins are receiving for the development of novel bioinspired materials (d'Ischia, Napolitano, Pezzella, Meredith & Buehler, 2020; Manini et al. 2019), including applications in food technology (Roy & Rhim, 2021).

Besides, inhibition of melanin biosynthesis also has distinct importance. Human skin hyperpigmentation, melasma and photo-induced dyschromia are consequences of dysregulated melanin biosynthesis (Nicolaidou & Katsambas, 2014). Therefore, inhibition of biosynthesis has been a long-term goal in biomedical and cosmetic science (Panzella & Napolitano, 2019).

Although formed from different phenolic precursors as compared to skin melanin, production of melanin-type pigments in food gives rise to a dark color (enzymatic browning), accompanied by other deterioration processes such as changes of flavor, unpleasant odor and loss of nutritional value, especially during postharvest processing and storage of vegetables and fruits (Moon, Kwon, Lee & Kim, 2020). Since the level of melanin is mainly regulated by tyrosinase activity, its inhibition has become a prominent strategy in food preservation (Martínez-Alvarez Lopez-Caballero, Montero & del Carmen Gomez-Guillen, 2020; Song, Ni, Zhang, Zhang, Pan & Gong, 2021; Yu & Fan, 2021; Shao et al., 2018), paralleling the importance of inhibiting autoxidation and microbial spoilage (Moon, et al., 2020).

Tyrosinase (EC 1.14.18.1), a polyphenol oxidase (PPO), is ubiquitous (Nawaz et al., 2017) and has a highly-conserved type III copper center in the active site (Olivares & Solano, 2009). It is involved in two consecutive yet different oxidative catalytic cycles: the *ortho*-hydroxylation of

monophenols (*e.g.* L-tyrosine) by oxygen to *o*-diphenols (monophenolase reaction) and the oxidation of *o*-diphenols (*e.g.* L-DOPA) by oxygen to *o*-quinones (diphenolase activity) (Mondal, Thampi & Puranik, 2018). Quinones then undergo further spontaneous reactions leading to melanin (Figure 1). Tyrosinase inhibitors are most often assayed spectrophotometrically, using well established and convenient mushroom tyrosinase (mTY) (Shao et al. 2018), which is incubated with L-tyrosine or L-DOPA as the natural substrates to selectively monitor, respectively, monophenolase or diphenolase reaction. Both reactions are monitored from the growth in absorbance at 475 nm due to the subsequent spontaneous formation of colored dopachrome (DC), as schematized in Figure 1. Although the method is very well established and convenient, it is not free from errors. For instance, it relies on the detection of a late product. Additionally, other molecules (*e.g.* when testing extracts as inhibitors) could absorb at 475 nm or be transformed to afford colored intermediates that might interfere with the spectrophotometric reading (Mayr et al., 2019). Since oxygen is an obliged reactant in both monophenolase and diphenolase cycles and its total consumption is stoichiometrically related to the total formation of products (Naish-Byfield & Riley, 1992), we set to develop a method of real-time monitoring of the kinetics of oxygen consumption during tyrosinase reaction, by means of a miniaturized sensor based on near infrared (NIR) fluorescence quenching. The approach steps from the extensive experience of our group in monitoring the kinetics of oxygen uptake in oxidative radical reactions (Guo, Baschieri, Amorati & Valgimigli, 2021; Haidasz et al., 2016). Our hypothesis was that it would well match with the conventional spectrophotometric monitoring of dopachrome formation and afford a convenient and highly reliable combined method to investigate tyrosinase kinetics and inhibition.

To date, a large number of compounds with tyrosinase inhibition activity, of synthetic or natural origin, have been discovered (Zolghadri, et al, 2019); among them, certainly glabridin stands out. Originally extracted from licorice roots (*Glycyrrhiza glabra*, L.) it was the first *G. glabra* phytochemical with confirmed anti-tyrosinase activity, and the most potent (Nerya, Vaya, Musa, Izrael, Ben-Arie, & Tamir, 2003). It was later found also in other botanical sources, and reported as

one of the most active natural mTY inhibitors, with 15-folds higher activity than kojic acid (Yamauchi, Mitsunaga & Batubara, 2011), more effective than resveratrol and oxyresveratrol (Wang et al., 2018). Owing to its potency glabridin has been taken as drug lead to develop novel synthetic inhibitors (Jirawattanapong, Saifah, & Patarapanich, 2009), while pharmaceutical/food-grade licorice extracts standardized in glabridin (*e.g.* 40%) have become commercially available (Tamura, 2017). Nonetheless, the literature on its actual activity is quite confusing: IC_{50} values of 5.25, 2.93, 0.77 and 0.09 μM have been reported for inhibition of mTY with substrate L-tyrosine (Nerya et al, 2003; Yamauchi et al., 2011; Kim, Seo, Lee, Lee, 2005; Li, Li, Zhu, Lai, & Wu, 2021), spanning about two orders of magnitude. There is only one complete kinetic study addressing the mechanism of mTY inhibition, which was reported as noncompetitive both for monophenolase and diphenolase reactions, with Michaelis-Menten (M-M) inhibition constants K_I of 0.38 mM and 0.81 mM, respectively (Nerya et al, 2003). These surprisingly high values are at odds with the reported IC_{50} values, and with the much lower K_I values available for reportedly less effective inhibitors like kojic acid (K_I in the range 18-23 μM for monophenolase activity) (Kim, Yun, Lee, Lee, Min & Kim, 2002) – it should be recalled that lower values indicate higher activity. Therefore, our hypothesis was that glabridin's activity would require revision.

Given its importance, we re-investigated the activity of glabridin on mTY as a test-bench for our new oxygen uptake kinetic approach, using kojic acid as reference inhibitor. Hence, the scope of our study was first to set-up and validate our novel kinetic approach and, second, to afford revised mechanism and kinetics for glabridin, as a key reference for future studies and applications.

<Figure 1 about here>

2. Materials and methods

2.1 Materials

Glabridin (≥ 98%), L-tyrosine (≥ 98%), L-DOPA (3,4-dihydroxy-L-phenylalanine; ≥ 98%), kojic acid (5-Hydroxy-2-hydroxymethyl-4H-4-pyranone; ≥ 98.5%), water, acetonitrile and methanol (HPLC

grade) were purchased from Sigma-Aldrich (Milan, Italy). Commercial mushroom tyrosinase (EC 1.14.18.1, activity = 3130 units/mg) was purchased from Sigma-Aldrich and used without further purification. Fresh solutions were prepared twice a week in potassium phosphate buffer solution (50 mM, pH 6.8) and stored in small aliquots at -20°C for daily use. Given the difficulty to maintain the enzyme activity, tyrosinase activity was analysed spectrophotometrically every day during the experimental period, in order to adjust solutions to fixed tyrosinase Sigma units for consistent results. Briefly, one Sigma unit corresponds to the amount that will cause an increase in absorbance at 280 nm of 0.001 per minute at pH 6.8 in a 3 mL reaction mixture containing L-tyrosine. Sigma units were used throughout this study. One Sigma unit corresponds to 1.65×10^{-4} international units (I.U.) for monophenolase activity and to 2.24×10^{-2} I.U. for diphenolase activity, as defined by Fenoll et al. (2002). All other reagents were analytical grade from Sigma-Aldrich-Fluka, Merck (Milan, Italy).

2.2 Kinetics studies by UV-vis spectrophotometry

Kinetic evaluation of monophenolase and diphenolase reaction of tyrosinase with or without inhibitor was carried out using UV-Vis spectrophotometry similarly to previous methods (Song et al., 2021; Chang et al., 2007), with modifications. Measurements were performed at 30°C in a Thermo Scientific (Milan, Italy) Biomate 5, equipped with a multi-cell changer coupled with a Heto DBT Hetotherm (Birkerød, Denmark) thermostatting water circulator for temperature control. The samples were analyzed in polystyrene low-volume cuvettes (1.5 mL, l = 1 cm, 12.5×12.5×45 mm). Absorbance of dopachrome was measured at 475 nm for a time-period of 20 to 60 min (1 scan / 55s) reading the solution against a reference cuvette containing all reaction components except the substrate, which was replaced with potassium phosphate buffer (50 mM, pH 6.8). Absorbance variation *vs* time at different substrate concentration allowed to obtain initial velocity ($V = \Delta A/\Delta min$) which was converted in µM/min according to Lambert-Beer law as follows: V (µM/min) = V ($\Delta A/\Delta min$) × 10^6 / $\varepsilon_{\lambda max}$× l. The molar extinction coefficient (ε) for dopachrome at λ_{max}= 475 nm is 3700 M^{-1} cm^{-1}. Michaelis-Menten parameters (K_m e V_{max}) were obtained by processing initial velocity

vs substrate concentration data by nonlinear fitting to M-M equation (1), using Sigmaplot 11.0 (Systat Software Inc., San Jose, California). Linearized Lineweaver-Burk equation (2) was instead used to help identify the inhibition mode (Copeland, 2000). In both equations, V indicates the measured initial rate of reaction (*vide supra*), [S] is the initial substrate concentration, while V_{max} and K_m are respectively the maximum reaction rate (at saturating substrate concentration) and the M-M constant (the substrate concentration yielding half-maximum reaction rate).

$$V = \frac{V_{max}\,[S]}{K_m + [S]} \quad (1)$$

$$\frac{1}{V} = \frac{K_m}{V_{max}\,[S]} + \frac{1}{V_{max}} \quad (2)$$

The effect of inhibitors on enzyme reaction was evaluated at fixed tyrosinase units (3.85 U/mL for L-DOPA, 7.70 U/ml for L-tyrosine) and varying substrate concentrations (6-7 levels of L-DOPA and L-tyrosine, from 0 to 1.2 mM and 0 to 1.0 mM respectively), testing reactions without and with glabridin (0 to 300 nM for diphenolase; 0 to 50 nM for monophenolase) or kojic acid (0 to 100 μM).

2.3 Kinetics studies by oximetry

Evaluation of tyrosinase monophenolase and diphenolase kinetics and inhibition by glabridin or kojic acid was carried out by monitoring the oxygen consumption, at 30°C, by a NIR (760-790 nm) fluorescence oxygen sensor contained in a stainless-steel needle, connected to a FireSting-O2 (2 channels, FSO2-2) meter via an optical fiber (Pyrosience GmbH, Bremen, Germany). The samples were contained in 2.4 mL glass flasks, which were hand-made by a local scientific glass blower, provided with a PTFE coated stirring bar, immersed in a water bath controlled by Heto DBT Hetotherm (Birkerød, Denmark) thermosetting unit, and equipped with a submersed sealed magnetic stirrer MixDrive 1 XS + Mix Control (2mag AG, Munchen, Germany). The equipment set-up is illustrated in the Appendix. The oxygen consumption was recorded every second, and all reaction components, except the inhibitor concentration, were maintained identical to those set for UV-vis spectrophotometry. The raw data collected directly from the oxygen sensor is a percentage (P) of the

saturating oxygen concentration in the sample, corresponding to 0.236 mM at 30°C which reflects in the sensor reading as 20% (P_0). Thus, the oxygen concentration during the time course of the enzymatic oxidation of L-DOPA or L-tyrosine were converted into mM by the following equation: $[O_2]$ (mM) = P × 0.236 (mM) / 20%. The initial rate of oxygen consumption was obtained by regression of the initial data range of oxygen consumption (ΔP) *vs* time (in seconds), as illustrated in representative Fig. S3 and Fig. S4 (see Appendix), and they were converted by equation: V (μM/min) = V (ΔP/Δt) × 0.236 × 10^3 × 60 / P_0 (see Appendix, Table. S1), which were used for further analysis by non-linear fitting to Michaelis-Menten kinetics (eq. 1). In order to match the kinetic of oxygen consumption and that of dopachrome formation assessed spectrophotometrically (see paragraph 2.2), the uninhibited reaction was monitored at different activity of the enzyme (1-25 U/mL) and fixed concentration of substrate (1.6 mM for both L-DOPA and L-tyrosine), or at fixed activity of the enzyme (7.70 U/mL or 3.85 U/mL) and variable concentration of substrate, in matched experiments, comparing the initial rates of dopachrome formation and oxygen consumption at 30°C.

2.4 Analysis of glabridin as a substrate of mushroom tyrosinase

To verify whether glabridin is a substrate of mTY, beside being an inhibitor, we performed a variant of the assay described by Mayr et al. (2019). Mushroom tyrosinase (mTY, 7.70 U/mL) was incubated in phosphate buffer (pH 6.8) at 30°C with glabridin 200 nM and 1 mM in the absence of other substrates, and the reaction was monitored either spectrophotometrically (full scan 200-600 nm) or by the oxygen sensor over 1 hour, to record any sign of reaction.

2.5 Statistical analysis

Each measurement was performed in triplicate. Values of V_{max} and V_{max}^{app}, and of K_m and K_m^{app} in the absence and presence of inhibitors were determined from non-linear regression of M-M plots based on 5 to 7 concentrations of the substrate, which were analysed by Shapiro-Wilk Test with significance set at $P \leq 0.05$. Results are expressed as regression value ± standard error.

3. Results and Discussion

3.1 Parallel monitoring of the tyrosinase reaction by oximetry and spectrophotometry

In order to study monophenolase and diphenolase activities of mTY, L-tyrosine or L-DOPA were used as substrate, respectively, following the *o*-hydroxylation of L-tyrosine to L-DOPA and its further oxidation to *o*-dopaquinone, or just the second step, taking advantage of the higher rate of the diphenolase reaction, which renders L-tyrosine hydroxylation rate-limiting when using it as the substrate. The reaction was first monitored spectrophotometrically following the formation of dopachrome (DC) at 475 nm at 30°C, according to the most established practice (Song et al, 2021; Shao et al., 2018). Measurements performed at fixed concentration of mTY and variable concentration of substrate afforded the typical sigmoidal kinetic profile, with an initial lag time when the substrate was L-tyrosine. Plotting the initial rate of DC formation versus the substrate concentration showed good M-M behavior (Figure 2A, C). Since tyrosinase activity is essentially an oxidation process operated by oxygen, where oxygen is directly involved into the production of late product DC, we set to improve the reliability of spectrophotometric measurements by parallel oximetry studies. In matched experiments performed in closed vials, we monitored the oxygen concentration as a function of time during the reaction progress, using a miniaturized oxygen sensor based on NIR fluorescence quenching (see Appendix for instrumental settings). Results are compared to those obtained by spectrophotometry in Figure 2 (plots B and D). It can be noted that the kinetic profile of oxygen consumption also follows the typical M-M behavior, being complementary to the formation of dopachrome and suggesting that both methods are suited to monitor the reaction kinetics.

<Figure 2 about here>

This result was expected, since oxygen is the obliged oxidant in both cycles and it can be kinetically regarded as a substrate of tyrosinase (Fenoll et al., 2001). Our result also well matches the pioneering work by Naish-Byfield & Riley (1992) showing Michaelis-Menten kinetic profiles of oxygen consumption (monitored electrochemically) during the oxidation of 4-hydroxyanisol by

mTY, and by Rodriguez-López et al. (Rodriguez-López, Ros-Martínez, Varón & García-Cánovas, 1992) who showed complementarity between oxygen consumption (monitored electrochemically) and product accumulation during the mTY oxidation of *tert*-butylcatechol.

3.2 Correlation of the stoichiometry of oxygen consumption to dopachrome formation

The stoichiometric ratios of oxygen consumption to dopachrome accumulation during mTY reaction for substrates L-tyrosine and L-DOPA were previously investigated, respectively, by Naish-Byfield & Riley (1992) and by Rodriguez-López et al. (1992) by electrochemical analysis (Clark electrode) of oxygen in the reaction mixture.

In our study, the stoichiometric ratio was determined from comparison of the initial rates of O_2 consumption to that of DC formation, for both substrates L-tyrosine and L-DOPA, in matched kinetic experiments with the two methods (Figure 3). We judged this approach more accurate than measuring the total oxygen consumption and product formation at the end of the reaction, since the further spontaneous transformation of DC (on the way to melanin) might influence the apparent DC absorbance at the later stages of enzyme reaction. Our results were in full agreement with previous findings that the stoichiometry of oxygen consumption depends on the substrate, being 1 mol O_2 : 1 mol of DC when the substrate is L-DOPA, and 1.5 mol of O_2 : 1 mol of DC when the substrate of L-tyrosine (Naish-Byfield & Riley,1992; Rodriguez-López et al.,1992).

This result agrees with the notation that 0.5 mol of O_2 is consumed to hydroxylate L-tyrosine to L-DOPA and another 0.5 mol of O_2 is needed to oxidize L-DOPA to dopaquinone. However, subsequent spontaneous cyclization forms cyclodopa (leukodopachrome) that is oxidized to dopachrome by rapid redox reaction with dopaquinone (Mondal et al., 2018), which is reduced back to L-DOPA. This last consumes another 0.5 mol of O_2 to be oxidized again to DOPAquinone (Naish-Byfield & Riley,1992; Rodriguez-López et al.,1992), as depicted in Figure 1.

Since it was reported that (for other substrates) the stoichiometry of oxygen consumption can vary with the experimental conditions, particularly with the concentration of enzyme and substrate (Peñalver, Hiner, Rodriguez-López, Garcıa-Canovas, & Tudela, 2002), we extended our correlation of the initial rates of reaction to a broad range of enzyme and substrate concentrations, by performing series of experiments at fixed substrate and variable enzyme activity and at fixed enzyme activity and variable substrate concertation, using both L-DOPA alone and L-tyrosine alone as the substrate. Results are summarized in Figure 3(C-F), and confirm that the stoichiometric ratio of oxygen consumption / dopachrome formation was 1.0±0.1 and 1.5±0.2 (O_2 to DC) for substrate L-DOPA and L-tyrosine, respectively, over the whole range of experimental settings.

<Figure 3 about here>

This result agrees with previous studies with L-tyrosine and L-DOPA (Naish-Byfield & Riley,1992; Rodriguez-López et al.,1992), but is at variance with a study in which *tert*-butylphenol (TBP) and *tert*-butylcatechol (TBC) where used, respectively, to assess oxygen consumption during monophenolase and diphenolase reaction, showing a variation of O_2/product stoichiometric ratio for very low substrate/enzyme concentration ratio (Peñalver et al., 2002). The different outcome is possibly due to the higher stability in solution of the products formed from TBP/TBC, as previously discussed in detail (Peñalver et al., 2002).

3.3 Validation of oxygen consumption kinetics on uninhibited activity of mTY

Upon establishing the actual stoichiometric ratio of oxygen consumption and dopachrome formation, the kinetic measurements performed by the two approaches could be compared on quantitative grounds. The initial rates of the reaction were analysed according to Michaelis-Menten equation and the K_m and V_{max} values for the monophenolase and diphenolase activity were obtained by non-linear regressions. For reaction with substrate L-tyrosine (monophenolase) K_m measured by

spectrophotometry and by O_2 sensing was 0.18±0.01 mM and 0.17±0.02 mM, respectively, while V_{max} was 9.01±0.12 µM/min and 8.45±0.62 µM/min, respectively. Instead, for substrate L-DOPA (diphenolase) K_m from spectrophotometry and O_2 sensing was 0.26±0.02 mM and 0.24±0.02 mM, respectively, while V_{max} was 25.80±0.53 µM/min and 24.18±0.96 µM/min, respectively (results are collected in Table S2 in Appendix)**.** It can be noted that the two kinetic approaches afford results in excellent agreement, being identical within experimental error. Our data also match well with previous literature, *e.g.* Ros et al. (Ros, Rodríguez-López, García-Cánovas, 1994) reported K_m of 0.168 mM and 0.272 mM respectively for monophenolase and diphenolase reaction, while Fenoll et al. (2001), in a very detailed study, reported K_m as 0.25 mM and 0.28 mM for the two reactions. This provides good validation of our real-time oxygen consumption approach to investigate tyrosinase kinetics.

3.4 Inhibition kinetics by Glabridin and Kojic Acid

Glabridin is claimed one of the most effective natural inhibitors of tyrosinase, but there is major uncertainty on its actual activity on quantitative grounds, in spite of its role as reference compound, as previously illustrated. Given its importance, we investigated its kinetic of inhibition addressing both monophenolase and diphenolase activities, by both methods (spectrophotometry and oxygen uptake) in matched studies. Results are summarized in Figure 4, in which non-linear fittings of M-M plots were used for quantitative analysis, while linear Lineweaver-Burk plots helped identify the mechanism. This choice aimed at increasing the accuracy, since obtaining V_{max} (and K_m) directly from the intercept in Lineweaver-Burk plots is subject to higher intrinsic error (Copeland, 2000).

<Figure 4 about here>

Literature on the activity profile of this molecule indicates a noncompetitive inhibitory mechanism (Nerya et al., 2003; Chen, Yu & Huang, 2016).), which implies that glabridin is capable of binding with the same affinity both the free enzyme (E) and the complex enzyme-substrate (ES). A kinetic consequence of this type of inhibition is that the apparent maximum reaction rate V_{max}

should decrease with the concentration of the inhibitor, while the apparent M-M constant K_m should remain unchanged (Copeland, 2000). However, both spectrophotometry and oximetry did not show noncompetitive but nearly competitive inhibition, as it can be judged from Lineweaver-Burk plots (eq. 2) in Figure 4 (C, D, G, H). In such plots the intercept on the Y-axis (= $1/V_{max}$) is nearly constant in the absence of the inhibitor or with different concentrations of glabridin, which implies that V_{max} does not depend on the concentration of glabridin, as it is expected for a competitive inhibitor. On the contrary, noncompetitive inhibitors should show an intercept on the Y-axis which increases with the concentration of the inhibitor. Additionally, the intercept on the X-axis (= $-1/K_m$) becomes less negative on increasing the concentration of glabridin, meaning that K_m is increasing, which is typical of competitive inhibitors.

The activity of a competitive inhibitor is best quantified by the M-M derived inhibition constant K_I, which represents the dissociation constant of the Enzyme-Inhibitor (EI) complex (eq 1), hence the smaller the value the higher the inhibition. Since a closer inspection of Lineweaver-Burk plots shows some minor variation of V_{max} particularly in oxygen uptake plots (Figure 4 G, H), to a first judgment, inhibition by glabridin was considered of mixed-type. Mixed-type inhibitors interfere with both the free enzyme and enzyme-substrate (ES) complex, with two (different) dissociation constants K_I and K_{SI} (eqs 3, 4), the first relating to the inhibitor bonded to the free enzyme and the other indicating the inhibitor bonded to the ES complex. Noncompetitive inhibitors would show $K_I = K_{SI}$.

$$K_I = \frac{[E][I]}{[EI]} \quad (3)$$

$$K_{SI} = \frac{[ES][I]}{[ESI]} \quad (4)$$

To determine K_I and K_{SI} for a mixed-type inhibition from M-M kinetic treatment, it is useful to introduce the parameters α and an α', which are given as follows:

$$\alpha = \frac{K_m^{app}}{K_m}\alpha' \quad (5)$$

$$\alpha' = \frac{V_{max}}{V_{max}^{app}} \quad (6)$$

Here K_m and K_m^{app} are respectively the M-M constant (substrate concentration giving half-maximum rate) in the absence and in the presence of the inhibitor, and V_{max} and V_{max}^{app} are respectively the maximum rate measured in the absence and in the presence of the inhibitor. K_I and K_{SI} values were then obtained from eqs. 7 and 8 at each concentration of the inhibitor [I].

$$\alpha = 1 + \left(\frac{[I]}{K_I}\right) \quad (7)$$

$$\alpha' = 1 + \left(\frac{[I]}{K_{SI}}\right) \quad (8)$$

The kinetics parameters determined for inhibition by glabridin (from data in figure 4), both with L-tyrosine and L-DOPA, by monitoring both DC formation and O_2 uptake, are listed in Table 1.

Table 1. Kinetic parameters of tyrosinase activity inhibition by glabridin at 30°C (pH = 6.8). Kinetic data were obtained by non-linear fitting of M-M plots at different glabridin concentrations.[a]

A. Kinetic parameters of tyrosinase diphenolase activity inhibition by glabridin.

	Dopachrome (DC) formation				Oxygen (O_2) consumption [a]			average
[Glabrindin] (nM)	0	90	180	300	0	80	200	
V_{max} or V_{max}^{app} (μM/min)	25.80 ±1.53	24.81 ±1.14	22.74 ±2.52	20.04 ± 4.32	24.18 ±0.96	22.50 ± 1.32	19.66 ±1.26	
K_m or K_m^{app} (mM)	0.26 ±0.02	0.67 ±0.06	1.08 ±0.02	1.31 ±0.46	0.21 ±0.02	0.47 ±0.08	0.66 ±0.05	
$\alpha = (K_m^{app} \times \alpha') / K_m$		2.63	4.79	6.65		2.34	3.87	
$\alpha' = V_{max} / V_{max}^{app}$		1.04	1.13	1.29		1.08	1.23	
$K_I = [I]/(\alpha-1)$ (nM)		55.21	47.54	53.10		59.86	69.68	57.08 ±8.32
$K_{SI} = [I]/(\alpha'-1)$ (nM)		2250.40	1337.72	1034.48		1071.42	869.57	1312.72 ±550.43

B. Kinetic parameters of tyrosinase monophenolase activity inhibition by glabridin.

	Dopachrome (DC) formation				Oxygen (O_2) consumption [a]			average
[Glabrindin] (nM)	0	15	37	50	0	20	40	
V_{max} or V_{max}^{app} (μM/min)	9.00 ±0.12	8.26 ±0.60	7.80 ±0.24	7.56 ±1.20	8.4 ±0.06	7.92 ±1.20	7.62 ±1.38	
K_m or K_m^{app} (mM)	0.18 ±0.01	0.29 ±0.04	0.61 ±0.03	0.97 ±0.20	0.17 ±0.02	0.39 ±0.06	0.65 ±0.08	
$\alpha = (K_m^{app} \times \alpha')/K_m$		1.78	3.86	6.25		2.43	4.21	
$\alpha' = V_{max} / V_{max}^{app}$		1.09	1.15	1.19		1.06	1.10	
$K_I = [I]/(\alpha-1)$ (nM)		19.23	12.95	9.53		13.99	12.46	13.63 ±3.54
$K_{SI} = [I]/(\alpha'-1)$ (nM)		166.67	239.81	267.42		333.34	400.30	281.51 ±89.34

[a] V_{max} or V_{max}^{app} refer to not inhibited and inhibited assays, respectively, and K_m or K_m^{app} refer to not inhibited and inhibited assays, respectively. Data were obtained both by UV-vis spectrophotometry and by oximetry. V_{max} or V_{max}^{app} were calibrated by using the stoichiometry ratio of 1.5 for O_2/DC with substrate L-tyrosine and of 1.0 for O_2/DC with substrate L-DOPA.

Glabridin shows very potent activity in inhibiting both monophenolase and diphenolase reactions already at nanomolar concentration. Notably, spectrophotometry and oximetry afford results in excellent agreement, despite the major difference between the techniques. Both show only minor variation of V_{max} in the presence of the inhibitor, which becomes noticeable only at the highest concentrations, while K_m grows significantly with glabridin's concentration. This provides confirmation of the proposed mechanism (*vide supra*). Given the excellent agreement between results from spectrophotometry and oximetry, the two sets of data were combined. Concerning the mechanism of inhibition, it is also interesting to note that K_{SI}, quantifying the inhibition based on

interaction of glabridin (I) with the ES complex, is on average over 20-folds larger than K_I, describing the competitive inhibition (interaction of I with E), both for monophenolase and diphenolase activity. This roughly indicates that less than 5% the inhibition by glabridin is due to binding to ES *i.e.* to uncompetitive behavior. For most of its activity glabridin competes with substrate (L-tyrosine or L-DOPA) for the enzyme's active site in a classical competitive mode with K_I values of 13.63±3.54 nM and 57.08±8.32 nM, respectively. This is at variance with the previously reported mechanism. Most notably, the absolute values of K_I are four orders of magnitude lower than previously reported (!) for inhibition of mTY monophenolase and diphenolase reactions (Nerya et al, 2003), indicating much higher activity and supporting the reputation of glabridin as one of the most potent natural mTY inhibitors.

To validate our kinetic measurements, particularly in the light of the major difference with previous literature, we extended the study to kojic acid, which is often used as reference inhibitor. As expected, kojic acid afforded good inhibition at micromolar concentration, with excellent agreement between the kinetics of DC formation and O_2 consumption. Both methods converged showing mixed type inhibition when the substrate was L-dopa with K_I and K_{SI} values of 9.91±1.42 µM and 20.97±5.23 µM, respectively, while inhibition is nearly competitive with L-tyrosine, with K_I = 10.91±0.99 µM (see Figure S5 S6 and Table S3 in Appendix for full details) in good agreement with previous literature (Chen, Wei, Rolle, Otwell, Balaban, & Marshall, 1991; Kim et al, 2002; Deri et al., 2016).

Values measured here support the reportedly much higher activity of glabridin, which outperforms kojic acid by 3 orders of magnitude for monophenolase inhibition and by 2 orders of magnitude for diphenolase inhibition.

3.5 Determination of IC_{50} (half-maximal inhibitory concentration)

In enzymology, inhibitors are usually described in terms of inhibition type and inhibition constant, as we have discussed in the foregoing. This is the most valuable approach since it has a clear connection with the inhibitory mechanism and offers quantitative kinetic bases, allowing full comparison among different inhibitors and lab-to-lab transferability. However, enzyme inhibition is of crucial importance also in pharmacology and in other disciplines, where focus is more on the consequences of inhibition than on its mechanism. Therefore, it is most common to see the inhibition performance being reported in the literature as IC_{50} values. The IC_{50} indicates the concentration of an inhibitor that is able reduce the rate of enzyme reaction to 50% the value observed in the absence of the inhibitor, under the same conditions. A dose-response diagram is used to track the effect of inhibitors on the initial rate of enzymatic reaction at a fixed concentration of substrate, according to Langmuir isotherm equation (eq. 9) (Copeland, 2000).

$$\frac{V_I}{V_0} = \frac{1}{1+\frac{[I]}{IC_{50}}} \qquad (9)$$

The IC_{50} values of glabridin mTY inhibition against substrates L-tyrosine and L-DOPA at different substrate concentration are reported in Table S4 (Appendix). It is clearly possible to see the positive correlation between the IC_{50} value and the concentration of substrates (see Figure 5), as it is expected for inhibitors which are not purely noncompetitive (Copeland, 2000). Once again, the agreement between values obtained by spectrophotometric monitoring of DC and those from oxygen uptake kinetics was excellent, therefore they were averaged to afford more robust reference data (Table S4 and Figures S7 and S8 in Appendix). A similar behaviour was recorded for kojic acid (see Table S5 and Figures S9 and S10 in Appendix). The dependence on experimental settings somewhat limits the usefulness of IC_{50} in quantifying inhibitors' performance; thus, they were determined here mainly as a reference to compare with current literature. IC_{50} values measured for kojic acid, were in good agreement with previous literature *e.g.* they were respectively 32.8±6.5 μM and 17.0±3.4 μM for monophenolase and diphenolase activity with 1 mM substrate (see Table S5 for full data set) *vs*

reference 54 and 58 μM, respectively, with 1.8 mM substrate (Chang, Ding, Tai & Wu, 2007) or 12.24 μM against 0.7 mM L-tyrosine (Shao et al, 2018), and 19.2 against 0.5 mM L-DOPA (Song et al. 2021). Instead, for glabridin, the IC_{50} measured with both substrates (L-tyrosine and L-DOPA) are significantly smaller, compared to most literature data, which already contradict each-other spanning over orders of magnitude: *e.g.* 2.93 μM against 1 mM tyrosine and 25.5 μM against 6 mM DOPA (Yamauchi et al. 2011) to 0.09 μM against 1.2 mM tyrosine and 3.9 μM against 7 mM DOPA (Nerya et al. 2003).

<Figure 5 about here>

At 1 mM substrate the IC_{50} values for glabridin, averaged between O_2 sensing and spectrophotometry, were 79.5±6.9 nM and 257.0±12.7 nM, respectively, for monophenolase and diphenolase activities. Hence, they agree with Nerya et al. (2003) only for inhibition of monophenolase activity. For competitive inhibitors (or nearly competitive, like glabridin) the Cheng and Prusoff's linear correlation described by eq. 10 is expected between the IC_{50} and the concentration of substrate (Copeland, 2000), therefore a plot of IC_{50} *vs* [S] should have intercept on the Y-axis corresponding to K_I. Plots of Figure 5 have intercepts at 12 nM and 60 nM (spectrophotometry), and 14 nM and 65 nM (O_2 uptake), while the plots from averaged data (Figures S7 and S8) intercept the Y-axis at 13 nM and 62 nM for monophenolase and diphenolase inhibition, hence they are fully consistent with the K_I values for glabridin (independently determined from non-linear M-M fittings) reported in Table 1, standing for the reliability of our current measurements.

$$IC_{50} = K_I + \frac{K_I\,[S]}{K_m} \qquad (10)$$

Interestingly, our IC_{50} values for glabridin are two-three orders of magnitude lower than values recorded for kojic acid, for monophenolase-diphenolase inhibition, again supporting the reputation of glabridin as one of the most effective natural tyrosinase inhibitors.

3.6 Is glabridin a substrate for mTY?

Several molecules with reported anti-tyrosinase activity have also been found to act as alternative substrates for mTY. This is because mTY is a polyphenol oxidase (PPO) enzyme with no strict specificity for only one substrate. Particularly, inhibitors with a relevant ability to access the enzyme's active site (*e.g.* competitive inhibitors), with a non-hindered phenolic or polyphenolic structure, might act as alternative substrates. For instance, this is the case for catechins (Seo, Sharma, & Sharma, 2003) caffeic acid, ferulic acid, neohesperidin and other phenolic compounds (Mayr et al. 2019). Transformation of the inhibitor could form species with a UV-Vis spectrum able to interfere with the detection of dopachrome, and it would cause a decrease of the effective inhibitor's concentration, hence it could cause artefacts in the kinetic analysis of tyrosinase inhibition (Mayr et al. 2019). Since glabridin is a phenolic compound, it cannot be excluded that it also acts as alternative substrate and, to the best of our knowledge, this has never been assessed before. Incubation of mTY with glabridin in the absence of other substrates showed no development of absorbance at 475 nm or in the UV-Vis region when monitored spectrophotometrically (see Figure S11 in Appendix). This standard method (Mayr et al. 2019) rules out interference in the spectrophotometrically measured enzyme kinetics (see section 3.3), but it does not provide a conclusive proof of the absence of reaction, as it relies on the formation of persistent, intensely absorbing products. To this end, we repeated the incubation of mTY with glabridin 200 nM or 1 mM, under identical conditions used in the assays, in the absence of L-tyrosine or L-DOPA, and monitored the reaction by our oxygen sensing method, recording no oxygen uptake over 60 min (see Figure S12 in Appendix). Since the two tested concentrations of glabridin correspond, respectively, to the highest level it was employed as inhibitor and the highest concentration used for the natural substrate tyrosine, the absence of any detectable reaction allows to exclude that glabridin acts as alternative substrate under our testing conditions. This study also illustrates the distinctive usefulness of our real-time oxygen sensing approach.

4. Conclusions and perspective

A new method to investigate kinetics and inhibition of tyrosinase activity was described. It is based on real-time sensing of oxygen via miniaturized NIR fluorescence probes, and showed to be practical and reliable to investigate tyrosinase inhibition. When it was matched to the conventional spectrophotometric approach, it proved to afford identical results. On the other hand, it offers higher versatility, as it does not rely on the formation of specific products with characteristic UV-Vis absorption. Therefore, it might prove of great value also to investigate the formation of allomelanins. Its setup and operation is much simpler than other methods to analyse oxygen consumption in solution, such as differential pressure transduction or electrochemical detection (Matera et al., 2015), which makes it an ideal complement of conventional spectrophotometric approaches to improve robustness and reliability in the study of tyrosinase inhibition, thereby favouring investigation in food science.

With the help of this method, accurate quantitative analysis on the anti-tyrosinase activity of glabridin were enabled, which prompted a revision of previously reported mechanism and kinetics. Current results indicate that mTY inhibition by glabridin is of mixed type, with prevailing competitive behavior both against substrate L-tyrosine and L-DOPA, affording, revised K_I values as 13.6 nM and 57.1 nM, for monophenolase and diphenolase inhibition, *i.e.* four orders of magnitude lower than previously reported. These results, along with revised IC_{50} values in the nanomolar range (80 nM and 294 nM, respectively, at 1 mM substrate) allow settling the long-standing controversy on the actual potency of this reference inhibitor, landing full support to the reputation of glabridin as one of the most potent natural tyrosinase inhibitors, and offering a solid reference for future investigations in food science.

Declaration of interest

The authors declare no competing financial interest.

Acknowledgments

This work was supported by a grant from the University of Bologna. Y.G. acknowledges a fellowship from China Scolarship Council (CSC201706790016). The authors thank Prof. Riccardo Amorati for access to the oximetry equipment.

Appendix A. Supplementary data

Detailed description of instrument set-up and operation, tables and graphs of mTY inhibition by Kojic acid, tables and plots of IC_{50} values for glabridin and kojic acid, UV-Vis spectra and O_2 uptake plots of glabridin incubated with mTY. Supplementary data associated with this article can be found, in the online version, at …

References

Chang, T.-S., Ding, H.-Y., Tai, S. S.-K., & Wu, C.-Y. (2007). Mushroom tyrosinase inhibitory effects of isoflavones isolated from soygerm koji fermented with Aspergillus oryzae BCRC 32288. *Food Chemistry*, *105*, 1430–1438. doi:10.1016/j.foodchem.2007.05.019

Chen, J. S., Wei, C.-I., Rolle, R. S., Otwell, W. S., Balaban, M. O., & Marshall, M. R. (1991). Inhibitory effect of kojic acid on some plant and crustacean polyphenol oxidases. *J. Agric. Food. Chem.*, *39*, 1396-1401.

Chen, J., Yu, X., Huang, Y. (2016). Inhibitory mechanisms of glabridin on tyrosinase. *Spectrochimica Acta Part A: Molecular and Biomolecular Spectroscopy*, *168*, 111–117. http://dx.doi.org/10.1016/j.saa.2016.06.008

Copeland, R. A. (2000). *Enzymes: A Practical Introduction to Structure, Mechanism, and Data Analysis*, (2nd Ed.), New York: Wiley-VCH. ISBN: 0-471-22063-9.

d'Ischia, M., Napolitano, A., Pezzella, A., Meredith, P. & Buehler, M. (2020). Melanin Biopolymers: Tailoring Chemical Complexity for Materials Design. *Angewandte Chemie International Edition*, *59*, 11196-11205. https://doi.org/10.1002/anie.201914276

d′Ischia, M., Wakamatsu, K., Cicoira, F., Di Mauro, E., Garcia-Borron, J.-C., Commo, S., Galvan, I., Ghanem, G., Kenzo, K., Meredith, P., et al. (2015). Melanins and melanogenesis:

483 from pigment cells to human health and technological applications. *Pigm. Cell*
484 *Melanoma Res.*, *28*, 520 – 544. https://doi.org/10.1111/pcmr.12393.

485 Deri, B., Kanteev, M., Goldfeder, M., Lecina, D., Guallar, V., Adir, N., & Fishman, A. (2016). The
486 unravelling of the complex pattern of tyrosinase inhibition. *Scientific Reports*, *6*, 1-10.
487 DOI: 10.1038/srep34993.

488 Fenoll, L. G., Rodriguez-Lopez, J. N., Garcia-Molina, F., Garcìa-Canovas, F. & Tudela, J. (2002).
489 Unification for the Expression of the Monophenolase and Diphenolase Activities of
490 Tyrosinase. *IUBMB Life*, *54*, 137–141. https://doi.org/10.1080/15216540214537

491 Fenoll, L. G., Rodriguez-Lopez, J. N., Garcia-Sevilla, F., Garcia-Ruiz, P. A., Varon, R., Garcia-
492 Canovas, F., Tudela, J. (2001). Analysis and interpretation of the action mechanism of
493 mushroom tyrosinase on monophenols and diphenols generating highly unstable o-
494 quinones. *Biochimica et Biophysica Acta*, *1548*, 1-22. https://doi.org/10.1016/S0167-
495 4838(01)00207-2

496 Guo, Y., Baschieri, A., Amorati, R., & Valgimigli, L. (2021). Synergic antioxidant activity of γ-
497 terpinene with phenols and polyphenols enabled by hydroperoxyl radicals. *Food*
498 *Chemistry*, *345*, 128468. https://doi.org/10.1016/j.foodchem.2020.128468

499 Guo, Y., Baschieri, A., Mollica, F., Valgimigli, L., Cedrowski, J., Litwinienko, G., & Amorati, R.
500 (2021). Hydrogen Atom Transfer from HOO to ortho-Quinones Explains the
501 Antioxidant Activity of Polydopamine. *Angew. Chem. Int. Ed.*, *60*, 15220–15224.
502 doi.org/10.1002/anie.202101033

503 Haidasz, E.A., Meng, D., Amorati, R., Baschieri, A., Ingold, K.U., Valgimigli, L., & Pratt, D.A.
504 (2016). Acid Is Key to the Radical-Trapping Antioxidant Activity of Nitroxides.
505 *Journal of the American Chemical Society*, *138*, 5290 – 5298. 10.1021/jacs.6b00677

506 Jirawattanapong, W., Saifah, E. & Patarapanich, C. (2009). Synthesis of Glabridin Derivatives as
507 Tyrosinase Inhibitors. *Arch. Pharm. Res.*, *32*, 647-654.
508 DOI 10.1007/s12272-009-1501-x

509 Kim, H. J., Seo, S. H., Lee, B. G., & Lee, Y. S. (2005). Identification of tyrosinase inhibitors from
510 Glycyrrhiza uralensis. *Planta Medica*, *71*, 785-787. https://doi.org/10.1055/s-2005-
511 871232

512 Kim, Y. M., Yun, J., Lee, C.-K., Lee, H., Min, K. R., & Kim, Y. (2002). Oxyresveratrol and
513 Hydroxystilbene Compounds. Inhibitory effects on tyrosinase and mechanism of action.

514 *Journal of Biological Chemistry*, *277*, 16340–16344.
515 https://doi.org/10.1074/jbc.M200678200

516 Li, C.-X, Li, T.-H., Zhu, M., Lai, J., Wu, Z.-P. (2021) Pharmacological properties of glabridin (a
517 flavonoid extracted from licorice): A comprehensive review. *Journal of Functional*
518 *Foods*, *85*, 104638. https://doi.org/10.1016/j.jff.2021.104638.

519 Manini, P., Lino, V., Franchi, P., Gentile, G., Sibillano, T., Giannini, C., Picardi, E., Napolitano, A.,
520 Valgimigli, L., Chiappe, C., & d'Ischia, M. (2019). A Robust Fungal Allomelanin
521 Mimic: An Antioxidant and Potent π-Electron Donor with Free-Radical Properties that
522 can be Tuned by Ionic Liquids. *ChemPlusChem*, *84*, 1331 – 1337.
523 https://doi.org/10.1002/cplu.201900195

524 Martínez-Alvarez, O., Lopez-Caballero, M. E., Montero, P., & del Carmen Gomez-Guillen, M.
525 (2020). The effect of different melanosis-inhibiting blends on the quality of frozen deep
526 water rose shrimp (Parapenaeus longirostris). *Food Control, 109,* 106889.
527 https://doi.org/10.1016/j.foodcont.2019.106889.

528 Matera, R., Gabbanini, S., Berretti, S., Amorati, R., De Nicola, G. R., Iori, R., & Valgimigli, L.
529 (2015). Acylated anthocyanins from sprouts of Raphanus sativus cv. Sango: Isolation,
530 structure elucidation and antioxidant activity. *Food Chemistry, 166,* 397–406.
531 http://dx.doi.org/10.1016/j.foodchem.2014.06.056

532 Mayr, F., Sturm, S., Ganzera, M., Waltenberger, B., Martens, S., Schwaiger, S., Schuster, D. &
533 Stuppner, H. (2019). Mushroom Tyrosinase-Based Enzyme Inhibition Assays Are Not
534 Suitable for Bioactivity-Guided Fractionation of Extracts. *J. Nat. Prod.*, *82*, 136−147.
535 DOI: 10.1021/acs.jnatprod.8b00847

536 Mondal S., Thampi A., & Puranik M. (2018). Kinetics of Melanin Polymerization during
537 Enzymatic and Nonenzymatic Oxidation. *Journal of Physical Chemistry B*, *122*, 7,
538 2047–2063. https://doi.org/10.1021/acs.jpcb.7b07941

539 Moon, K. M., Kwon, E. B., Lee ,B., & Kim, C. Y. (2020). Recent Trends in Controlling the
540 Enzymatic Browning of Fruit and Vegetable Products. *Molecules*, *25*, 2754.
541 https://doi.org/10.3390/molecules25122754

542 Naish-Byfield, S., & Riley, P. A. (1992). Oxidation of monohydric phenol substrates by tyrosinase.
543 An oximetric study. *Biochemical Journal*, *288*, 63–67.
544 https://doi.org/10.1042/bj2880063

Nawaz, A., Shafi, T., Khaliq, A., Mukhtar, H., & ul Haq, I. (2017). Tyrosinase: Sources, Structure and Applications. *International Journal of biotechnology & bioengineering*, *5*,142-148. https://doi.org/10.25141/2475-3432-2017-5.0135

Nerya, O., Vaya, J., Musa, R., Izrael, S., Ben-Arie, R., & Tamir, S. (2003). Glabrene and isoliquiritigenin as tyrosinase inhibitors from licorice roots. *Journal of Agricultural Food Chemistry*, *26*, 1201-1207. https://doi.org/10.1021/jf020935u

Nicolaidou, E. & Katsambas, A. D. (2014). Pigmentation disorders: hyperpigmentation and hypopigmentation. *Clinics in Dermatology*, *32*, 66-72. https://doi.org/10.1016/j.clindermatol.2013.05.026

Olivares, C., & Solano, F. (2009). New insights into the active site structure and catalytic mechanism of tyrosinase and its related proteins. *Pigment Cell & Melanoma Research*, *22*, 750-760. https://doi.org/10.1111/j.1755-148X.2009.00636.x

Panzella, L. & Napolitano, A. (2019). Natural and Bioinspired Phenolic Compounds as Tyrosinase Inhibitors for the Treatment of Skin Hyperpigmentation: Recent Advances. *Cosmetics*, *6*, 57. https://doi.org/10.3390/cosmetics6040057

Peñalver, M. J., Hiner, A. N. P., Rodriguez-López, J. N., Garcıa-Canovas, F., & Tudela J. (2002). Mechanistic implications of variable stoichiometries of oxygen consumption during tyrosinase catalyzed oxidation of monophenols and o-diphenols. *Journal Biochimica et Biophysica Acta (BBA)- Protein Structure and Molecular Enzymology 1597*, 140-148. https://doi.org/10.1016/S0167-4838(02)00264-9

Rodriguez-López, J. N., Ros-Martínez, J. R., Varón, R., & García-Cánovas, F. (1992). Calibration of a Clark-type oxygen electrode by tyrosinase-catalyzed oxidation of 4-tert-butylcatechol. *Analytical Biochemistry*, *202*, 356-360. https://doi.org/10.1016/0003-2697(92)90118-Q

Ros, J. R., Rodríguez-López, J. N., García-Cánovas, F. (1994). Tyrosinase: kinetic analysis of the transient phase and the steady state, *Journal Biochimica et Biophysica Acta (BBA) - Protein Structure and Molecular Enzymology*, *1204*, 33-42. https://doi.org/10.1016/0167-4838(94)90029-9

Roy, S. & Rhim, J.-W. (2021) New insight into melanin for food packaging and biotechnology applications. *Critical Reviews in Food Science and Nutrition*, 1-27 https://doi.org/10.1080/10408398.2021.1878097

576 Seo, S.-Y., Sharma, V. K., & Sharma, N. (2003). Mushroom Tyrosinase: Recent Prospects *J. Agric.*
577 *Food Chem.*, *51*, 2837−2853.

578 Shao, L.-L., Wang, X.-L. Chen, K., Dong, X.-W., Kong, L.-M., Zhao, D.-Y., Hider, R. C., & Zhou,
579 T. (2018). Novel hydroxypyridinone derivatives containing an oxime ether moiety:
580 Synthesis, inhibition on mushroom tyrosinase and application in antibrowning of fresh-
581 cut apples. *Food Chemistry*, *242*, 174–181.
582 http://dx.doi.org/10.1016/j.foodchem.2017.09.054

583 Song, X , Ni, M., Zhang, Y., Zhang, G., Pan, J., & Gong, D. (2021). Comparing the inhibitory
584 abilities of epigallocatechin-3-gallate and gallocatechin gallate against tyrosinase and
585 their combined effects with kojic acid. *Food Chemistry, 349,* 129172.
586 https://doi.org/10.1016/j.foodchem.2021.129172

587 Tamura, Y. (2017). The History of Licorice Applications in Maruzen Pharmaceuticals Co., Ltd. In:
588 Sakagami, H. (Ed.*) Biological Activities and Action Mechanisms of Liquorice*
589 *Ingredients* (pp 13-35*).* London, UK: IntechOpen Ltd. ISBN: 978-953-51-3120-5.
590 http.//dx.doi.org/10.5772/65962.

591 Wang, Y., Hao, M.-M., Sun, Y., Wang, L.-F., Wang, H., Zhang, Y.-Z., Li, H.-Y., Zhuang, P.-W., &
592 Yang, Z. (2018) Synergistic Promotion on Tyrosinase Inhibition by Antioxidants.
593 *Molecules*, *23*, 106. doi:10.3390/molecules23010106

594 Yamauchi, K., Mitsunaga, T., & Batubara I. (2011). Isolation, identification and tyrosinase
595 inhibitory activities of the extractives from Allamanda cathartica. *Natural Resources*, *2,*
596 167-172. https://doi.org/10.4236/nr.2011.23022

597 Yu, Q. & Fan, L. (2021) Understanding the combined effect and inhibition mechanism of 4-
598 hydroxycinnamic acid and ferulic acid as tyrosinase inhibitors. *Food Chemistry, 352,*
599 129369. https://doi.org/10.1016/j.foodchem.2021.129369

600 Zolghadri, S., Bahrami, A., Tareq, M., Khan, H., Munoz-Munoz, J., Garcia-Molina, F., Garcia-
601 Canovas, F., & Saboury, A. A. (2019). A comprehensive review on tyrosinase
602 inhibitors. *Journal of Enzyme Inhibition and Medicinal Chemistry*, *34*, 279-309.
603 https://doi.org/10.1080/14756366.2018.1545767

604

605

606

Figures captions

Figure 1. (A) Oxidation of L-tyrosine and L-DOPA by oxygen catalysed by tyrosinase (TY), and (B) tyrosinase inhibitors investigated in this study.

Figure 2. Time-course of dopachrome (DC) production (A, C) and O_2 consumption (B, D) during the oxidation of L-dopa (A, B) and L-tyrosine (C, D) catalyzed by tyrosinase (3.85 U/ml for L-DOPA and 7.70 U/ml for L-tyrosine). The inserts are the initial rates of O_2 consumption and DC formation during the reaction fitted with Michaelis-Menten equation (solid lines).

Figure 3. (A, B) Representative traces of O_2 consumption (solid lines) and dopachrome (DC) formation (dashed lines) during the oxidation of L-DOPA 1.6 mM (A: tyrosinase 3.85 U/mL); and L-tyrosine 1.6 mM (B: tyrosinase 7.70 U/ml) at 30°C, pH 6.8. Regression lines were drawn using the indicated (red) time-range. (C-F) Correlation of the stoichiometry of O_2 consumption to dopachrome (DC) production during oxidation of L-tyrosine (A, B) and L-DOPA (C, D), as a function of: (A, C) tyrosinase concentration at fixed substrate, and (B, D) substrate concentration at fixed enzyme.

Figure 4. Kinetics of mTY inhibition by glabridin at 30°C (pH = 6.8): non-linear Michaelis-Menten fittings of diphenolase activity on L-DOPA (A, E) and of monophenolase activity on L-tyrosine (B, F), studied by UV-Vis spectrophotometry (A, B) and oximetry (E, F). C, D, G and H are the Lineweaver-Burk plots corresponding to A, B, C and D, respectively. Glabridin (Gla) concentrations are indicated by the corresponding symbols in the plots. Enzyme concentration for substrate L-dopa and L-tyrosine were 3.85 U/mL and 7.7U/mL respectively.

Figure 5. Dependency of IC_{50} for glabridin inhibition of mTY on substrate concentration, both for monophenolase (A) and diphenolase (B) reactions. Data (Table S4 in Appendix) were obtained both by spectrophotometry and by oxygen sensing at 30°C (pH= 6.8).

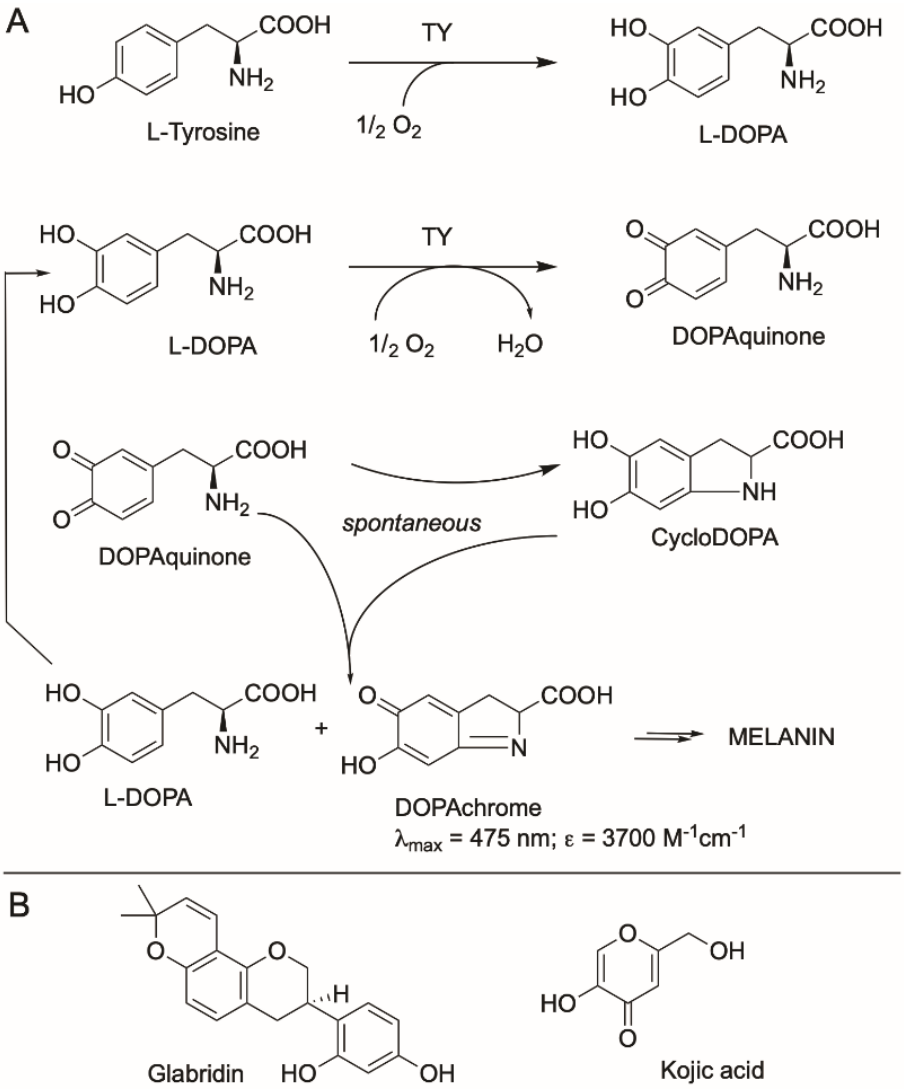

630

631 **Figure 1.** (A) Oxidation of L-tyrosine and L-DOPA by oxygen catalysed by tyrosinase (TY),

632 and (B) tyrosinase inhibitors investigated in this study.

633

634

635

636

637

638

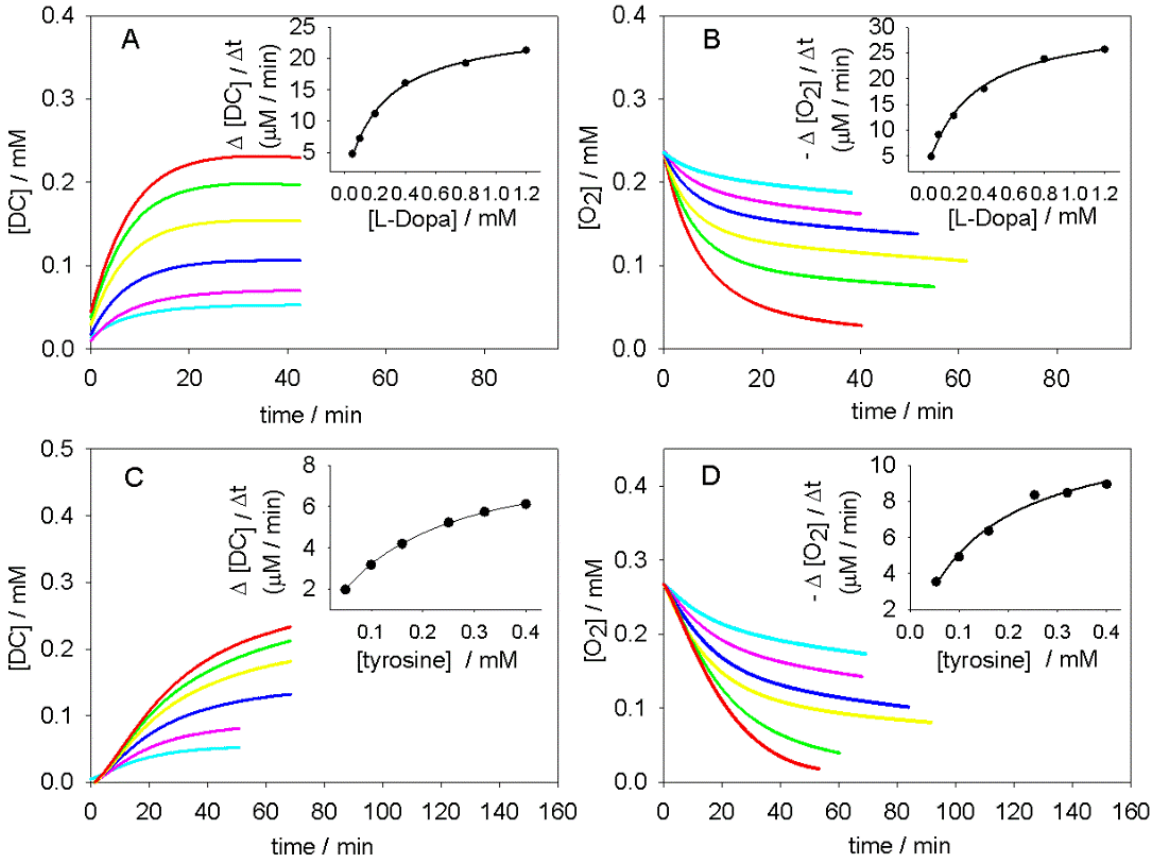

639

640 **Figure 2.** Time-course of dopachrome (DC) production (A, C) and O_2 consumption (B, D) during
641 the oxidation of L-dopa (A, B) and L-tyrosine (C, D) catalyzed by tyrosinase (3.85 U/ml for L-DOPA
642 and 7.70 U/ml for L-tyrosine). The inserts are the initial rates of O_2 consumption and DC formation
643 during the reaction fitted with Michaelis-Menten equation (solid lines).

644

645

646

647

648

649

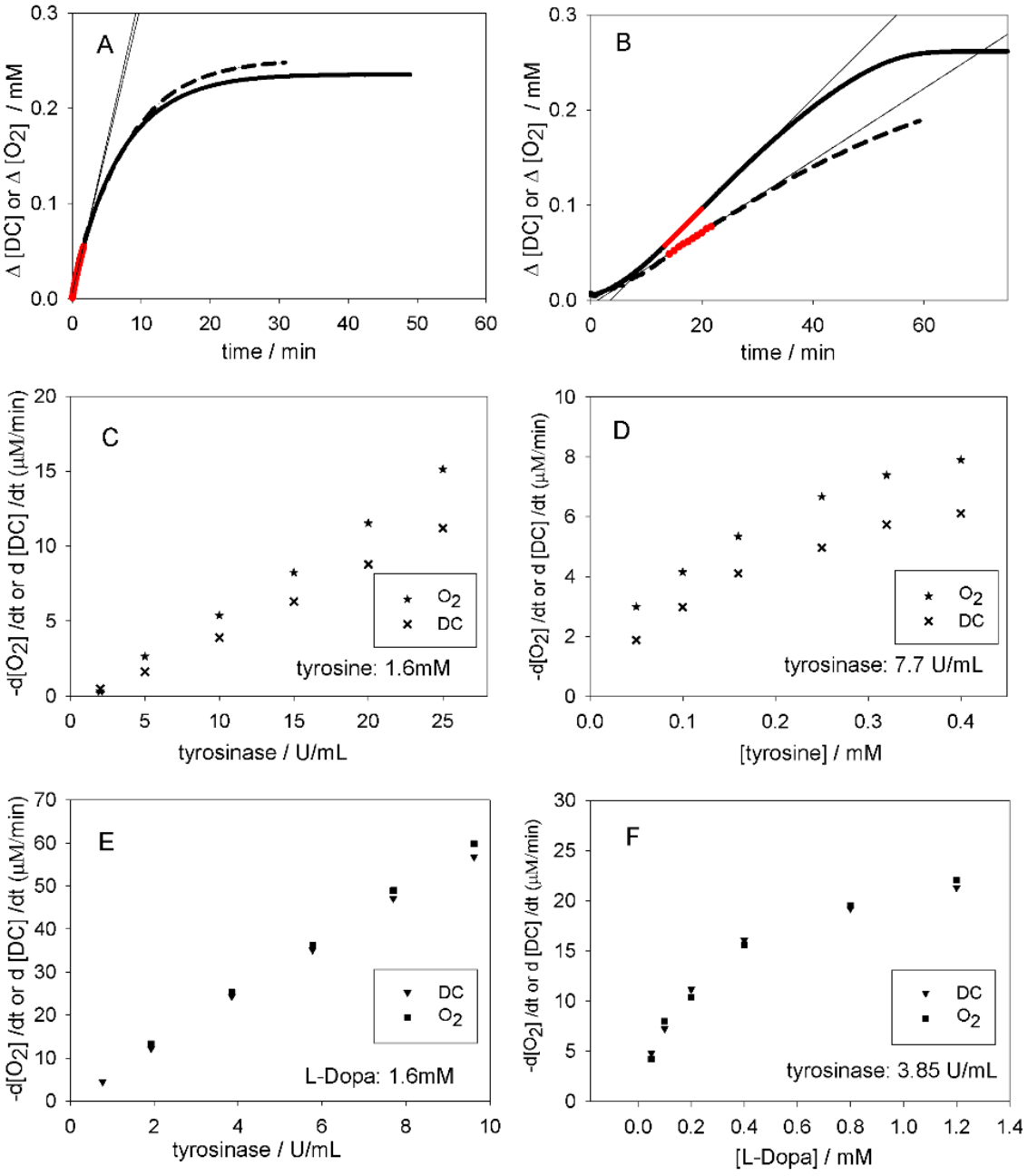

650

651 **Figure 3.** (A, B) Representative traces of O_2 consumption (solid lines) and dopachrome (DC)
652 formation (dashed lines) during the oxidation of L-DOPA 1.6 mM (A: tyrosinase 3.85 U/mL); and
653 L-tyrosine 1.6 mM (B: tyrosinase 7.70 U/ml) at 30°C, pH 6.8. Regression lines were drawn using the
654 indicated (red) time-range. (C-F) Correlation of the stoichiometry of O_2 consumption to dopachrome
655 (DC) production during oxidation of L-tyrosine (A, B) and L-DOPA (C, D), as a function of: (A, C)
656 tyrosinase concentration at fixed substrate, and (B, D) substrate concentration at fixed enzyme.

657

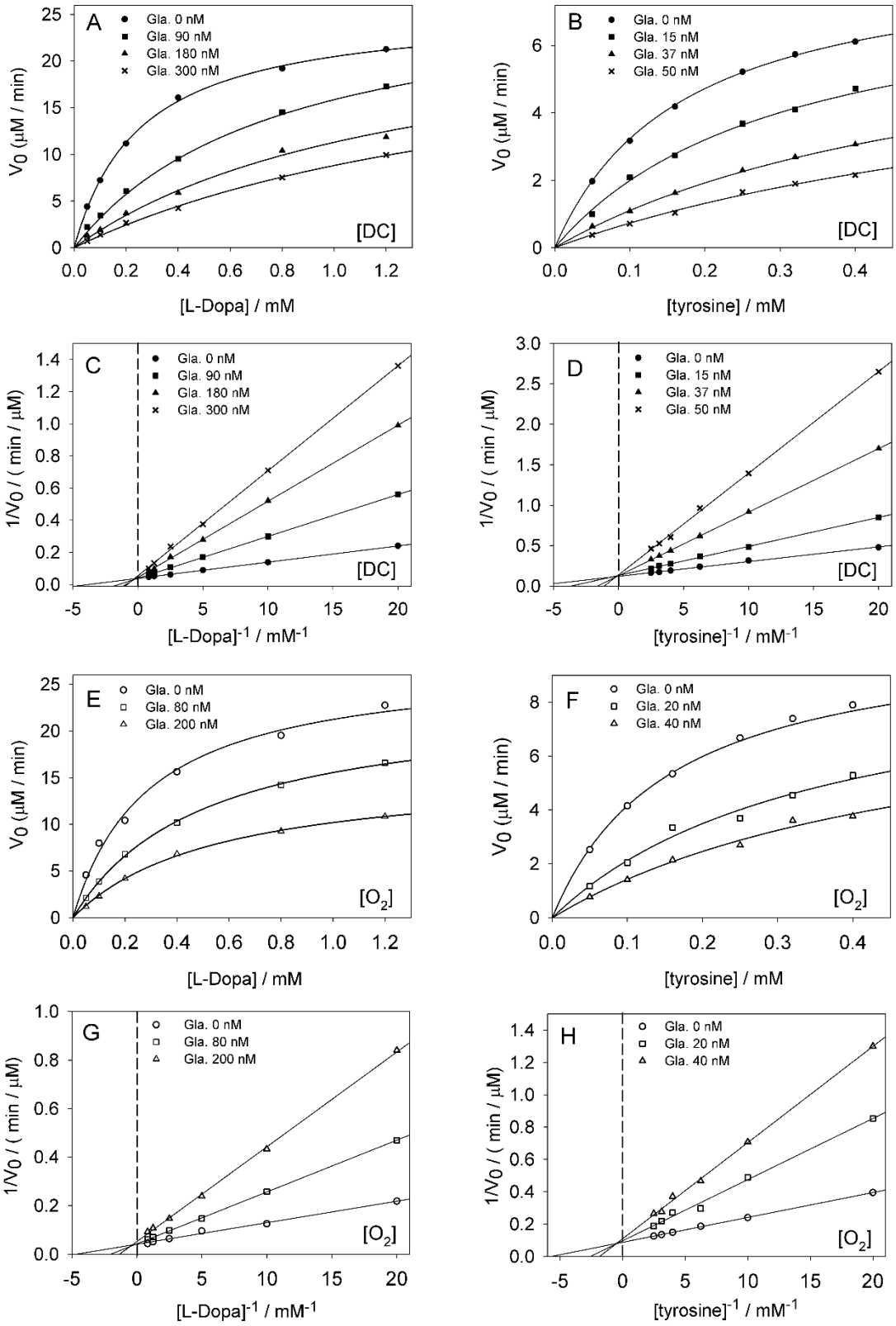

Figure 4. Kinetics of mTY inhibition by glabridin at 30°C (pH = 6.8): non-linear Michaelis-Menten fittings of diphenolase activity on L-DOPA (A, E) and of monophenolase activity on L-tyrosine (B, F), studied by UV-Vis spectrophotometry (A, B) and oximetry (E, F). C, D, G and H are the Lineweaver-Burk plots corresponding to A, B, C and D, respectively. Glabridin (Gla) concentrations are indicated by the corresponding symbols in the plots. Enzyme concentration for substrate L-DOPA and L-tyrosine were 3.85 U/mL and 7.7U/mL respectively.

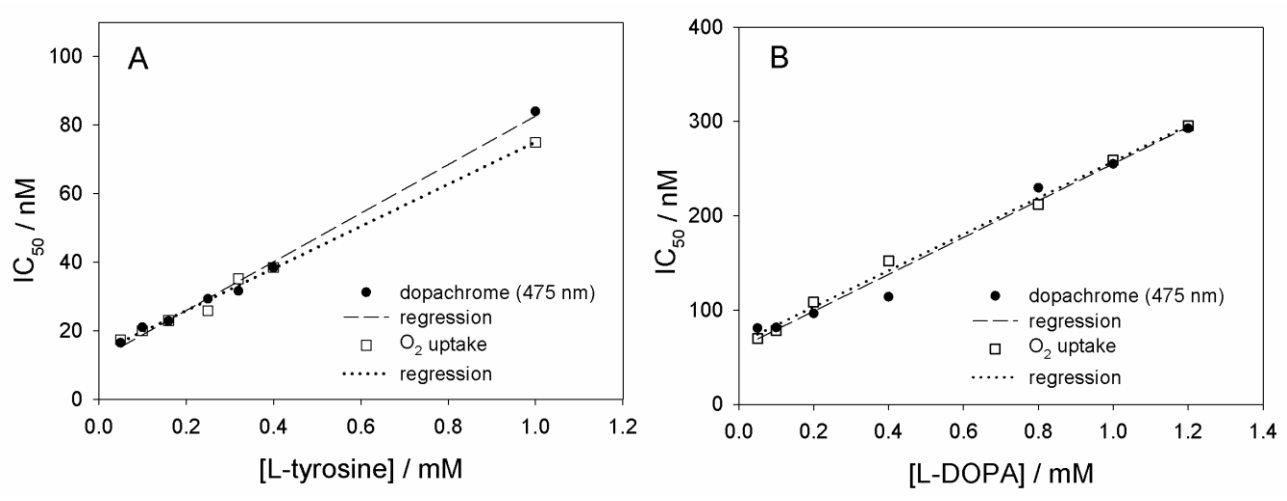

Figure 5. Dependency of IC_{50} for glabridin inhibition of mTY on substrate concentration, both for monophenolase (A) and diphenolase (B) reactions. Data (Table S4 in Appendix) were obtained both by spectrophotometry and by oxygen sensing at 30°C (pH= 6.8).

Real-time oxygen sensing as a powerful tool to investigate tyrosinase kinetics allows revising mechanism and activity of inhibition by glabridin

Yafang Guo,[a] Alice Cariola,[a] Riccardo Matera,[b] Simone Gabbanini,[b] & Luca Valgimigli*,[a]

[a] *University of Bologna, Department of Chemistry "G. Ciamician", Via S. Giacomo 1, 40126 Bologna, Italy;*

[b] *BeC s.r.l., R&D Division, Via C. Monteverdi 49, 47122 Forlì, Italy*

Appendix

Table of contents

Setup of the real-time oxygen sensing equipment

The equipment setup is illustrated in Figure S1.

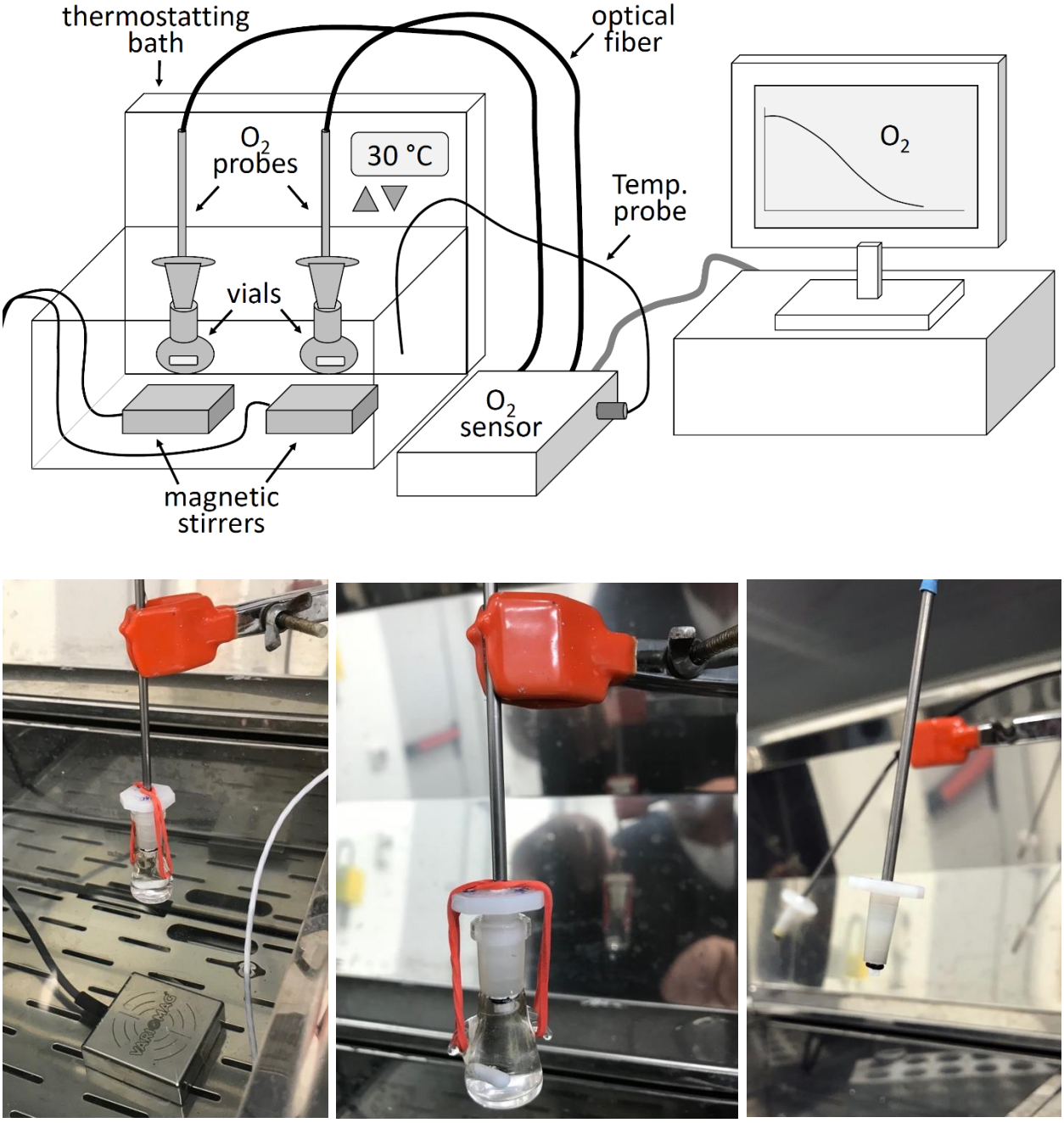

Figure S1. Scheme of the real-time oxygen sensing equipment (top) and images of the assembly of sample vials (int. volume 2.4 mL) with the oxygen probe sealed through the cap (bottom).

The equipment was set up using a commercial two channels Optical Oxygen Meter FireSting-O2 (model FSO2-2) connected via optical fibers to two IR fluorescence oxygen sensor probes (Robust type) contained in a 3 mm o.d. stainless-steel needle (Pyrosience GmbH, Bremen, Germany). The samples were contained in 2.4 mL glass flasks hand-made by a local scientific glass blower, sealed with a conical PP cap though which the O_2 sensor is inserted (after drilling the cap along the main axis) so that the sensor tip is protruding for about 3-4 mm inside the flask and is air-tight sealed. On closing the flask, care is taken to leave no air bubble, so that the entire volume is occupied by the (air-saturated) aqueous reaction mixture. The sample flask is provided with a PTFE-coated stirring bar and is completely submersed in a water bath controlled by Heto DBT Hetotherm (Birkerød, Denmark) thermosetting unit. Mixing is provided by submersed sealed magnetic stirrers MixDrive 1XS controlled by an external Mix Control (2mag AG, Munchen, Germany). The oxygen meter is connected to a temperature sensor (immersed in the water bath) for automatic correction of the sensor response, and to a PC via USB port for data collection.

Protection of the oxygen sensing probe form organic components

The O_2 sensor probes are designed and indicated by the manufacturer for use in aqueous solution, in the bare form, i.e. without any protection. Since the content in organic material in our samples was very limited, in principle the probes could be used, as indicated, without protection. However, on performing multiple measurements with the same probes, we noted a progressive loss in sensitivity with time, which we attributed to the deposition of thin layers of insoluble melanin on the surface of the polymeric matrix containing the fluorescent dye, in the sensor tip (only the lower surface is exposed to the solution, while the rest of the matrix is protected by the stainless-steel structure of the probe). Such loss of performance could not be overcome by accurate cleaning of the surface without causing damage to the probe itself. Therefore, we decided to protect the tip of the probe by coating with a polymeric membrane, which would allow sufficient permeability to oxygen to produce no interference with the kinetic measurements.

In order to protect the oxygen probe, several polymeric membranes were comparatively tested in reference kinetic assays for oxygen consumption, namely: 1) the time-course of oxygen concentration in a freshly prepared solution of 8 mM Na_2SO_3 in distilled water; 2) the autoxidation

of 10% (v/v) tetrahydrofurane (THF) in aqueous phosphate buffer (pH 7.4) initiated by the thermal decomposition of 50 mM azobisamidinopropane dihydrochloride (AAPH) at 30°C; 3) the autoxidation of 0.15% (w/v) soy lecithin in aqueous phosphate buffer (pH 7.4) initiated by 75 mM AAPH at 30°C. Tested membranes were: a) silicon 500 µm; b) LDPE 100 µm; c) LDPE 25 µm; d) LDPE/HDPE 12 µm; e) Teflon® (PTFE) 100 µm; f) Teflon® (PTFE) 76 µm. Among them, d) and f) offered the best compromise between oxygen permeability and mechanical properties: both offered no significant barrier to the consumption of oxygen at rates of ca. 0.1 mM/s, with measured rates of oxygen consumption differing less than ± 5% with respect to the bare (uncoated) probe. Teflon® (PTFE) 76 µm was selected for our kinetic measurements with tyrosinase for its inertness.

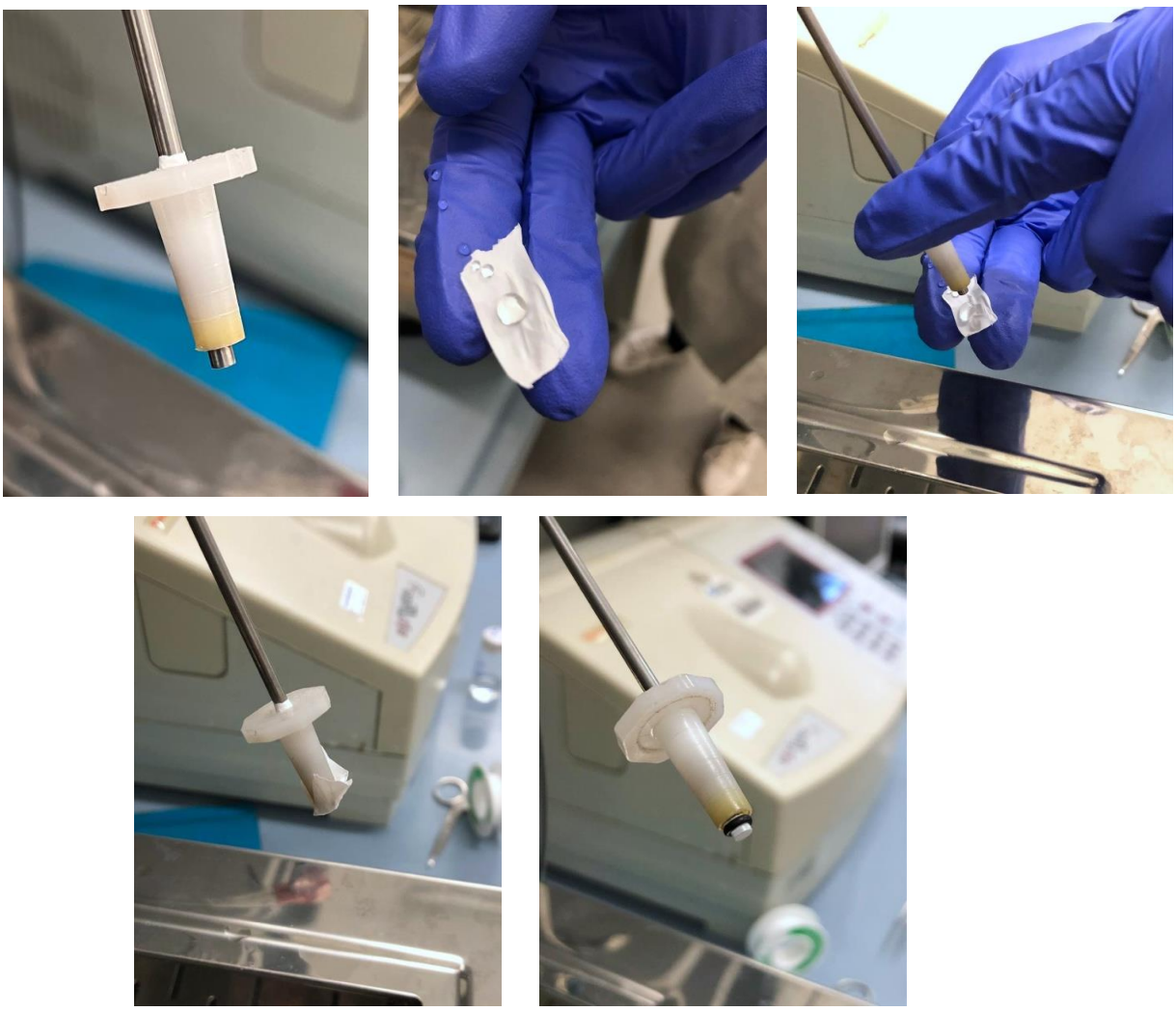

Figure S2. Stepwise procedure for coating the O_2 probe tip with a protective PTFE film (76 µM) held in place by an O-ring.

To guarantee reproducible measurements with no interference of the membrane, we found it is important to have both sides of the membrane "hydrated" *i.e.* in contact with water so that the diffusion of O_2 through the membrane follows the path water-membrane-water. To this end, we always took care of leaving a thin layer of buffered water (the same medium used for kinetic measurements) between the membrane and the lower (sensitive) surface of the oxygen probe. To do so, we applied a drop of buffer solution on the membrane and used it to obtain intimate adhesion of the membrane itself to the tip of the probe, then we fixed the membrane tightly in place with an O-ring, applied with the help of a micropipette tip (*e.g.* Gilson type), taking care of leaving no air bubble between the membrane and the tip of the probe, as illustrated in Figure S2. The membrane could be (gently) washed externally after every use and was replaced every day or every second day of experiments.

Measurements of mTY kinetics and inhibition

Oximetric evaluation of tyrosinase monophenolase and diphenolase kinetics was carried at 30°C by the real-time oxygen sensing equipment previously described. L-Tyrosine (0.05 – 1.0 mM) and L-DOPA (0.1 – 1.2 mM) were used, respectively as the substrate. Mushroom tyrosinase (3130 Units/mg; Sigma-Aldrich, Milan, Italy) solutions were prepared twice a week, stored at -20°C and checked on daily basis for activity, according to the manufacturer method (UV-Vis spectrophotometry), so to adjust dilution to the desired final activity. All activities were expressed in Sigma Units. The uninhibited reaction was monitored at different activity of the enzyme (1-25 U/mL). The raw data collected directly from the oxygen sensor is a percentage (P) of the oxygen saturation in the flask, corresponding to 0.236 mM at 30°C which reflects in the computer reading as 20%. Thus, the initial rate of the oxygen consumption (Table S1) was obtained by regression of the initial data range of oxygen consumption *vs* time using Sigmaplot software (Figure S3), upon converting the P value by the equation: $V\ (\mu M/s) = V\ (\Delta P\ /\Delta s) \times 0.236 \times 10^3 / P_0$ or $V\ (\mu M/min) = V\ (\Delta P\ /\Delta s) \times 0.236 \times 10^3 \times 60 / P_0$, as needed, to obtain the velocity in the desired units. In both equations P_0 is the oximetry reading value of the starting point, which usually is 20 after calibration of the oxygen sensor.

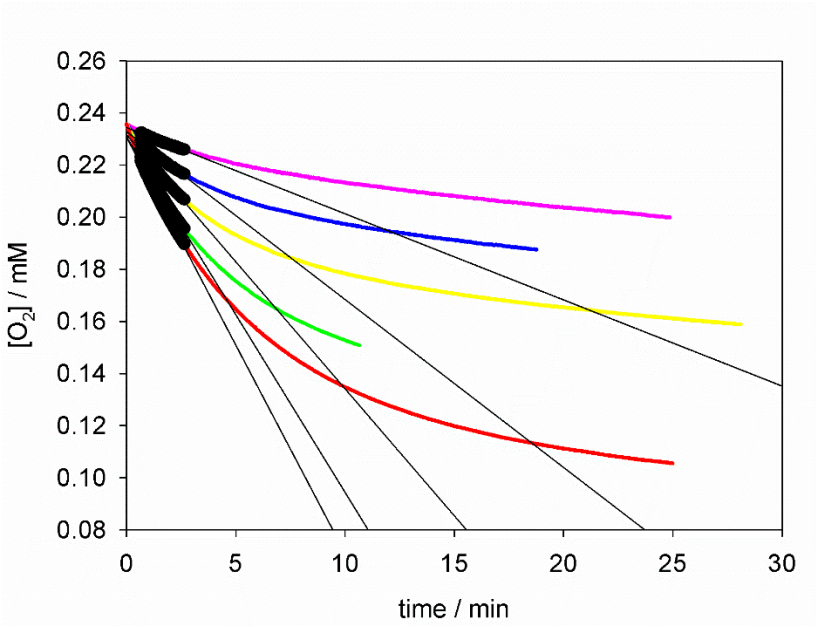

Figure S3. Example of time progresses of O_2 consumption during the oxidation of L-dopa at different initial concentration from 0.1 mM (purple line) to 1.2 mM (red line), inhibited by glabridin (80 nM). The black lines are the linear regression (*V*) for every L-dopa concentration, taken in the highlighted time range (40s to 160s).

Table S1. Example of rates obtained from the linear fitting by Sigamplot software of initial portions of oxygen consumption plots for different L-dopa concentrations (data from Figure S3).

[L-dopa] (mM)	0.1	0.2	0.4	0.8	1.2
V = slope of O_2 uptake (μM/min)	3.429	6.812	10.186	14.227	15.755

Initial velocity was plotted against the corresponding concentration of the substrate (*e.g.* L-dopa for diphenolase reaction) to obtain the Michaelis-Menten plot (Figure S4), which was analysed by non-linear regression. The non-linear analysis was conducted by fitting of experimental data point with the hyperbola equation $y = \frac{a\,x}{b + x}$ using sigmaplot software, where y, x, a and b represent V_0, [S], V_{max} and K_m respectively, for uninhibited kinetics, thereby representing M-M equation. An example of fitting results is shown in Figure S4.

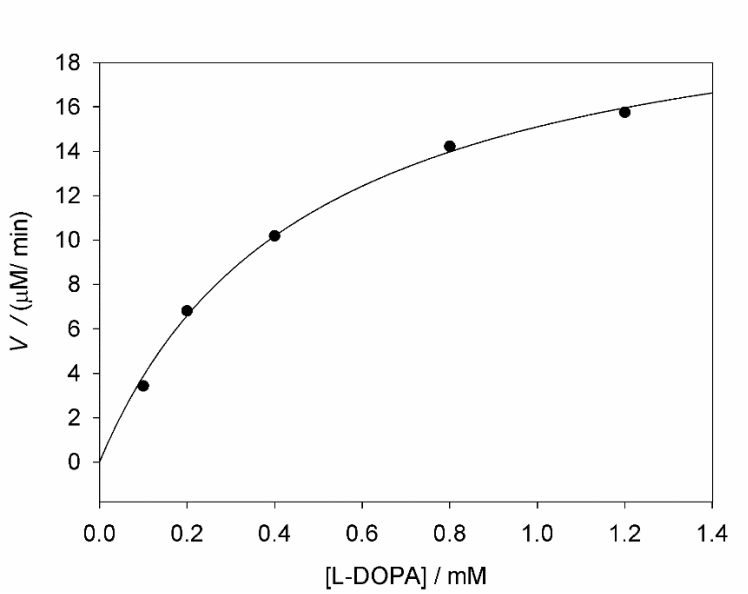

Figure S4. Example of plot of Initial rates of oxygen consumption during tyrosinase catalyzed oxidation of L-dopa and the corresponding non-linear fitting to Michaelis-Menten kinetics (data from Table S1).

Identical kinetic data collection and treatment was applied when using L-tyrosine as the substrate.

In this case the measured rate of O_2 consumption was divided by 1.5 to match with the rate of dopachrome (DC) formation, to account for the stoichiometric ratio of 1:1.5 of DC to O_2 for monophenolase reaction, as determined in matched kinetic measurements via the oxygen sensor and UV-Vis spectrophotometry (see main manuscript). No conversion was necessary for diphenolase reaction since the stoichiometric ratio DC to O_2 is 1:1.

For kinetic measurements in the presence of an inhibitor (Glabridin or Kojic acid), identical procedure was followed both for monophenolase and diphenolase reactions, using different concentrations of the inhibitor, for each set of measurements at different substrate concentration. In data treatment with equation $y = \frac{a\,x}{b + x}$, y, x, a and b represent V, [S], V_{max}^{app} and K_m^{app} respectively, where the last two are, respectively, the apparent V_{max} and K_m at each concentration of the inhibitor.

Table S2. Michaelis-Menten kinetics parameters measured both by UV-Vis spectrophotometry and by oximetry during uninhibited mushroom tyrosinase reaction at 30°C, pH=6.8.

		dopachrome formation		oxygen consumption	
activity	**substrate**	K_m **(mM)**	V_{max} **(μM/min)**	K_m **(mM)**	V_{max} **(μM/min)**
monophenolase	L-tyrosine	0.18±0.01	9.01±0.12	0.17±0.02	8.45±0.62
diphenolase	L-DOPA	0.26 ±0.02	25.80±0.53	0.24±0.02	24.18±0.96

Given the higher rate of the diphenolase reaction, the V_{max} of this process was calculated at the beginning of the process (between t=0 and t=3 min), while monophenolase activity was evaluated between 3 and 15 min, to skip the initial lag phase.

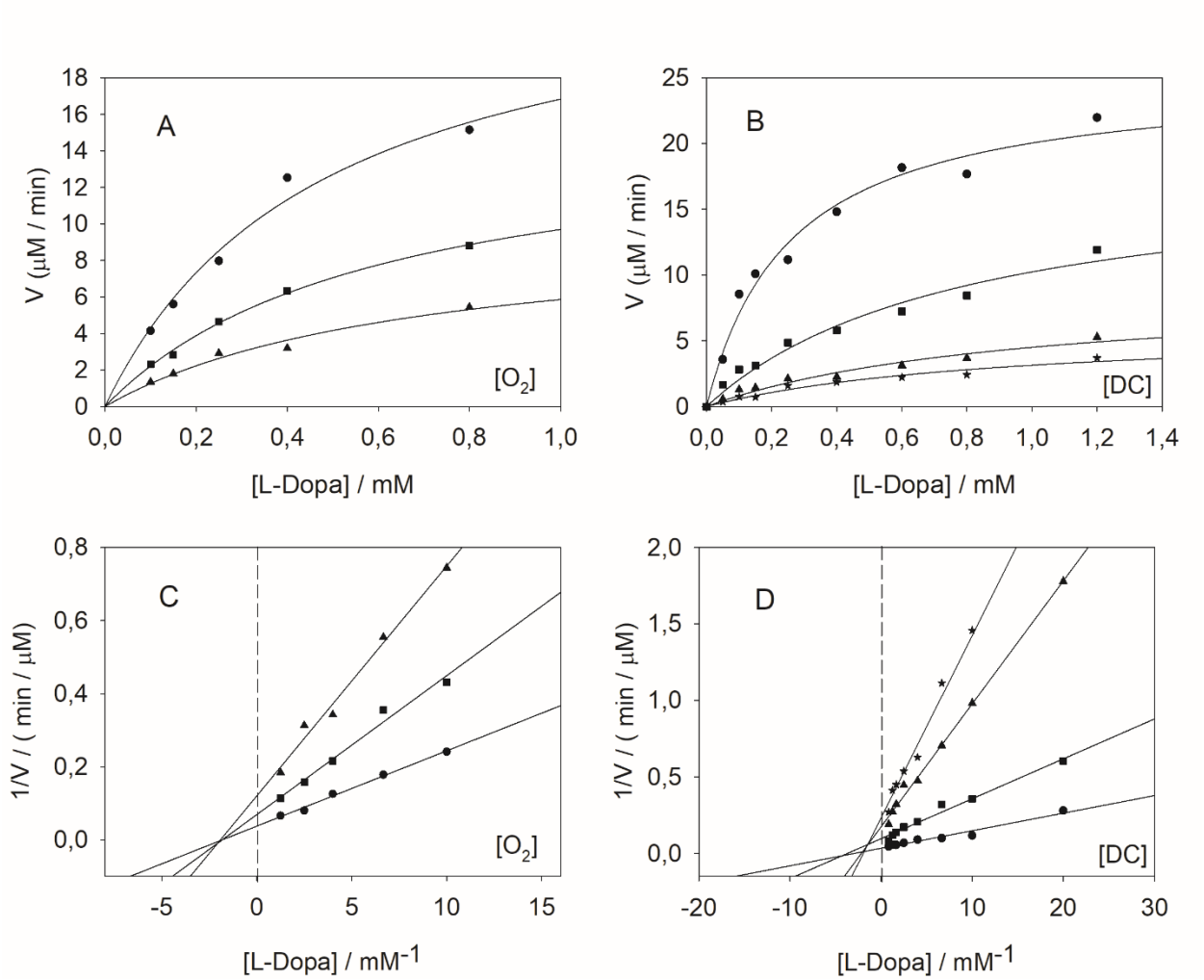

Figure S5. Non-linear fittings (A and B) of Michaelis-Menten kinetics for kojic acid inhibition of diphenolase tyrosinase activity and (C and D) the corresponding Lineweaver–Burk linear fittings. Data were obtained both by oximetry (A, C) and UV-Vis spectrophotometry (B, D): (A, C) kojic acid concentrations: ●-0 µM, ■- 20 µM, ▲-50 µM; (B, D) kojic acid concentrations: ●-0µM, ■-20 µM, ▲-50 µM, ★-100 µM. Enzyme concentration for substrate L-dopa was 3.85 U/ml, all experiments were conducted at pH 6.8 and 30°C. The rate of reaction *V* was evaluated from the initial portion (between t=0 and t=2 min) of the plot in each experiment.

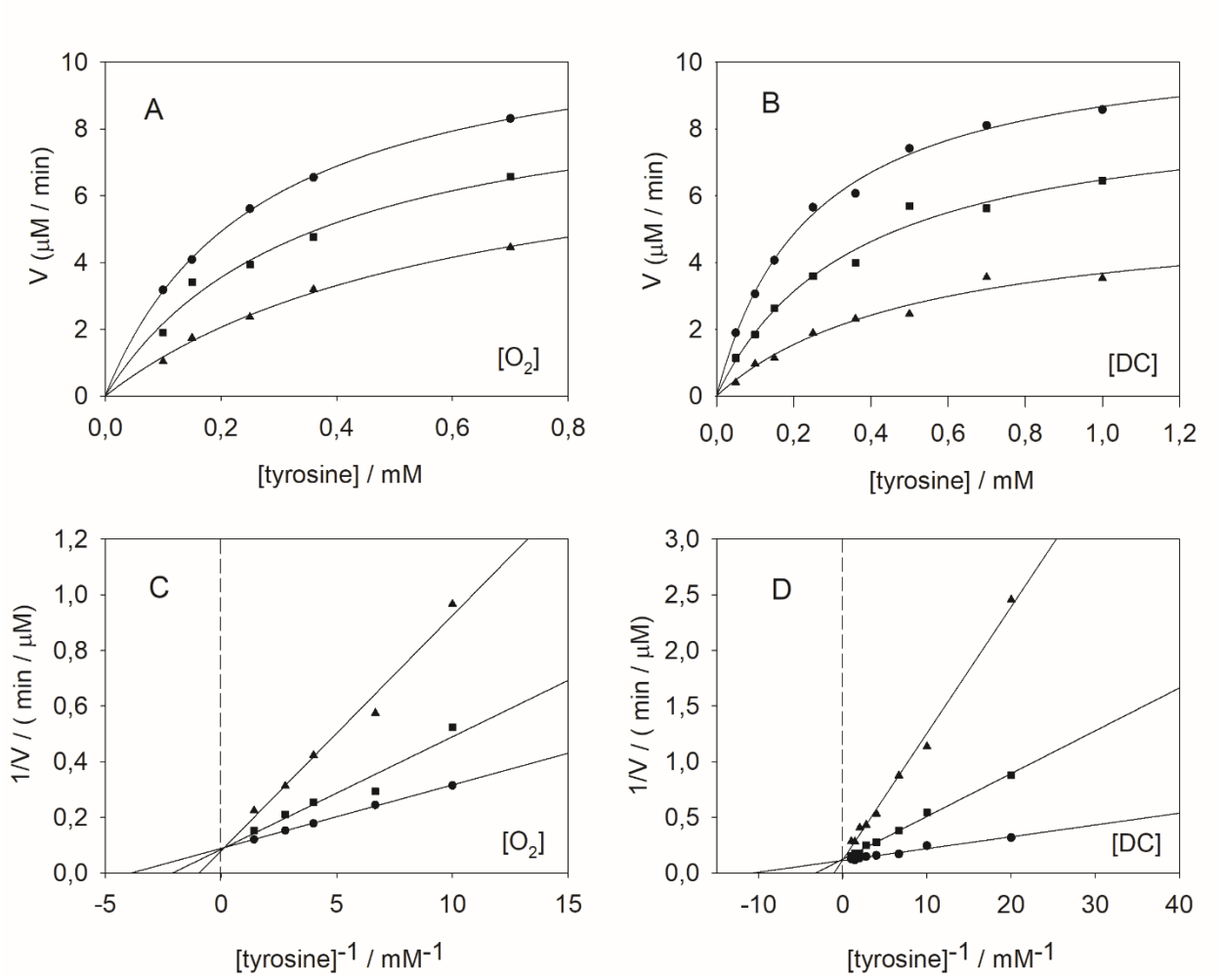

Figure S6. Non-linear fittings (A and B) of Michaelis-Menten kinetics for kojic acid inhibition of monophenolase tyrosinase activity and (C and D) the corresponding Lineweaver–Burk linear fittings. Data were obtained both by oximetry (A, C) and UV-Vis spectrophotometry (B, D): (A, C) kojic acid concentrations: ●-0 nM, ■- 16 µM, ▲-25 µM; (B,D) kojic acid concentrations: ●- 0 µM, ■- 10 µM, ▲- 30 µM. Enzyme concentration for substrate L-Tyrosine was 7.7 U/ml, all experiments were conducted at pH 6.8 and 30°C. The *V* of monophenolase activity was evaluated between 5 and 15 min.

Table S3. Kinetic parameters of tyrosinase activity inhibition by kojic acid at 30°C (pH= 6.8). Kinetics data were obtained by spectrophotometric monitoring of dopachrome (DC) or by real-time oxygen sensing (using the same procedure as for glabridin).

A. Kinetic parameters of tyrosinase diphenolase activity inhibition by kojic acid.								
	Dopachrome (DC) formation				Oxygen (O_2) consumption			Average
[kojic acid] (μM)	0	20	50	100	0	20	50	
V_{max} or V_{max}^{app} (μM/min)	30.66 ± 1.74	13.2 ± 2.76	7.38 ± 1.8	5.07 ± 0.12	23.82 ± 3.6	13.62 ± 0.96	8.28 ± 1.34	
K_m or K_m^{app} (mM)	0.26 ±0.05	0.34 ±0.02	0.47 ±0.04	0.53 ±0.03	0.28 ±0.01	0.45 ±0.07	0.52 ±0.02	
$\alpha = (K_m^{app} \times \alpha') / K_m$		2.98	7.42	12.26		2.77	5.35	
$\alpha' = V_{max} / V_{max}^{app}$		2.32	4.17	6.04		1.73	2.88	
$K_I = [I]/(\alpha-1)$ (μM)		10.08	7.79	8.89		11.30	11.50	**9.91 ±1.42**
$K_{I'} = [I]/(\alpha'-1)$ (μM)		15.12	15.79	19.85		27.48	26.62	**20.97 ±5.23**
B. Kinetic parameters of tyrosinase monophenolase activity inhibition by kojic acid.								
	Dopachrome (DC) formation			Oxygen (O_2) consumption [a]				Average
[kojic acid] (μM)	0	16	25	0	10	30		
V_{max} or V_{max}^{app} (μM/min)	8.94 ± 0.42	8.4 ± 0.66	7.98 ± 0.66	8.04 ± 0.96	7.5 ± 0.78	7.2 ± 0.48		
K_m or K_m^{app} (mM)	0.18 ± 0.02	0.36 ± 0.06	0.75 ± 0.12	0.26 ± 0.01	0.48 ± 0.09	1.07 ± 0.09		
$\alpha = (K_m^{app} \times \alpha')/K_m$		2.31	3.56		1.98	3.62		
$\alpha' = V_{max} / V_{max}^{app}$		1.06	1.12		1.07	1.12		
$K_I = [I]/(\alpha-1)$ (μM)		12.25	9.78		10.17	11.45		**10.91 ± 0.99**
$K_{I'} = [I]/(\alpha'-1)$ (μM)		266.67	208.33		142.85	250.00		**216.96 ± 55.16**

Note: V_{max} or V_{max}^{app} refer to not inhibited and inhibited assays, respectively, and K_m or K_m^{app} refer to not inhibited and inhibited assays, respectively. Data were obtained both by UV-vis spectrophotometry and by oximetry method. V_{max} or V_{max}^{app} were calibrated by using the stoichiometry ratios 1.5 for O_2/DC for monophenolase reaction and 1.0 O_2/DC for diphenolase.

Table S4. IC_{50} values calculated for mushroom tyrosinase inhibition by glabridin (at 30°C) at different concentrations of L-tyrosine and L-dopa substrates, both by spectrophotometric monitoring of dopachrome (at 475 nm) and by real-time oxygen sensing.

From UV-Vis. monitoring at 475 nm (diphenolase)							
[L-dopa] (mM)	0.05	0.10	0.20	0.40	0.80	**1.00**	1.20
IC_{50} (nM)	80.9	81.6	96.4	114.0	229.7	**255.1**	292.6
Error (±std.dev.)	±0.5	±3.5	±8.9	±10.1	±9.9	**±8.4**	±12.6
From real-time O_2 sensing (diphenolase)							
[L-dopa] (mM)	0.05	0.10	0.20	0.40	0.80	**1.00**	1.20
IC_{50} (nM)	69.8	78.4	108.3	152.4	201.1	**259.0**	295.7
Error (±std.dev.)	±0.6	±4.1	±10.5	±3.7	±3.3	**±15.7**	±33.4
Averaged between O_2 sensing and UV-Vis (diphenolase)							
[L-dopa] (mM)	0.05	0.10	0.20	0.40	0.80	**1.00**	1.20
IC_{50} (nM)	75.4	80.0	102.3	133.2	220.9	**257.0**	294.2
Error (±std.dev.)	±5.6	±4.1	±11.4	±20.6	±11.5	**±12.7**	±25.3
From UV-Vis. monitoring at 475 nm (monophenolase)							
[L-tyrosine] (mM)	0.05	0.10	0.16	0.25	0.32	0.40	**1.00**
IC_{50} (nM)	16.50	21.0	22.8	29.3	31.6	38.4	**84.0**
Error (±std.dev.)	±0.2	±0.8	±2.4	±2.4	±4.1	±3.9	**±6.9**
From real-time O_2 sensing (monophenolase)							
[L-tyrosine] (mM)	0.05	0.10	0.16	0.25	0.32	0.40	**1.00**
IC_{50} (nM)	17.4	20.0	23.0	25.9	35.2	38.5	**75.0**
Error (±std.dev.)	±0.2	±0.9	±4.9	±1.6	±4.3	±2.8	**±7.1**
Averaged between O_2 sensing and UV-Vis (monophenolase)							
[L-tyrosine] (mM)	0.05	0.10	0.16	0.25	0.32	0.40	**1.00**
IC_{50} (nM)	16.9	20.5	22.9	27.6	33.4	38.5	**79.5**
Error (±std.dev.)	±0.5	±1.0	±3.9	±2.7	±4.6	±3.4	**±8.3**

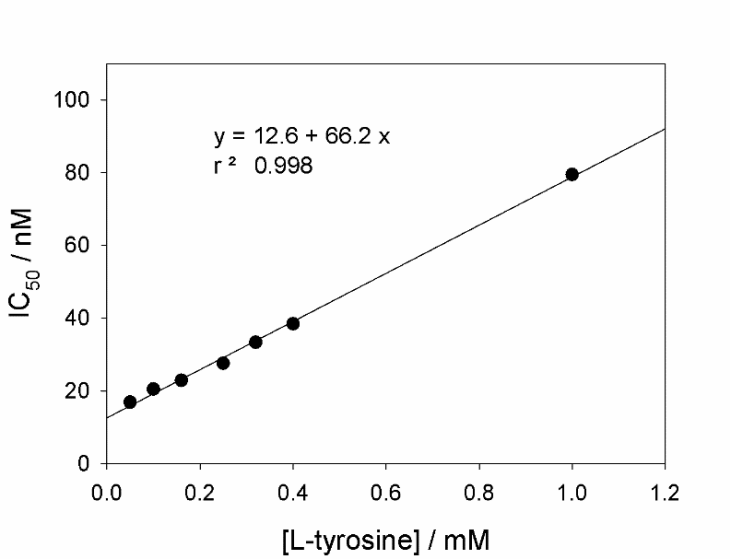

Figure S7. Dependency on the concentration of substrate of IC_{50} for glabridin in the inhibition of monophenolase activity of mushroom tyrosinase at 30°C (pH= 6.8), averaged between spectrophotometric monitoring of dopachrome and real-time O_2 sensing (data from Table S3).

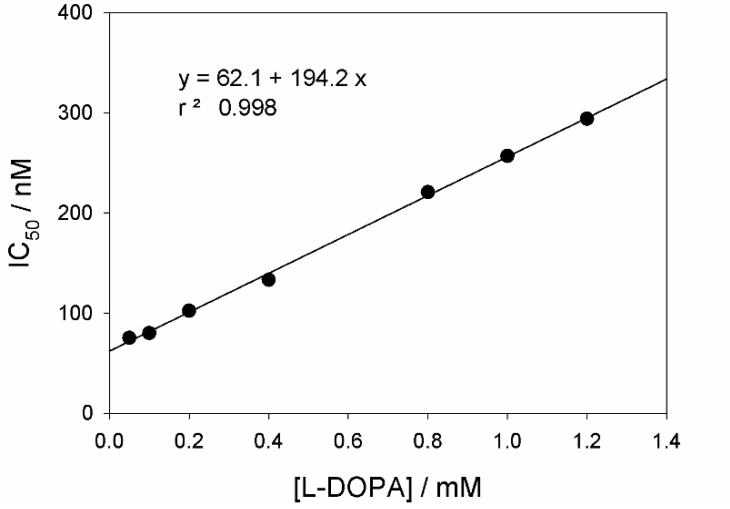

Figure S8. Dependency on the concentration of substrate of IC_{50} for glabridin in the inhibition of diphenolase activities of mushroom tyrosinase at 30°C (pH= 6.8), averaged between spectrophotometric monitoring of dopachrome and real-time O_2 sensing (data from Table S3).

Table S5. IC_{50} values calculated for mushroom tyrosinase inhibition by kojic acid (at 30°C; pH=6.8) at different concentrations of L-tyrosine and L-dopa substrates.

[L-dopa] (mM)	0.1	0.15	0.40	0.60	0.80	**1.00**	1.20
IC_{50} (μM)	9.4	8.3	12.1	12.5	15.8	**17.0**	19.9
Error (±std.dev.)	±2.1	±1.0	±2.7	±1.9	±2.6	**±3.4**	±3.9
[L-tyrosine] (mM)	0.05	0.10	0.15	0.25	0.36	0.7	**1.00**
IC_{50} (μM)	15.5	17.9	19.4	20.2	23.0	27.9	**32.8**
Error (±std.dev.)	±3.5	±2.9	±3.8	±2.4	±5.2	±4.4	**±6.5**

The IC_{50} were determined from combined data by averaging UV-Vis and O_2 uptake experiments.

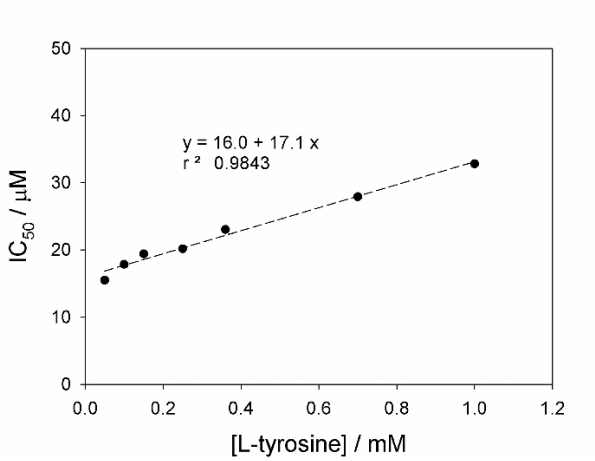

Figure S9. Plot of IC_{50} *vs* the concentration of substrate (L-Tyrosine) for monophenolase inhibition of mushroom tyrosinase by Kojic acid at 30°C (data from Table S4).

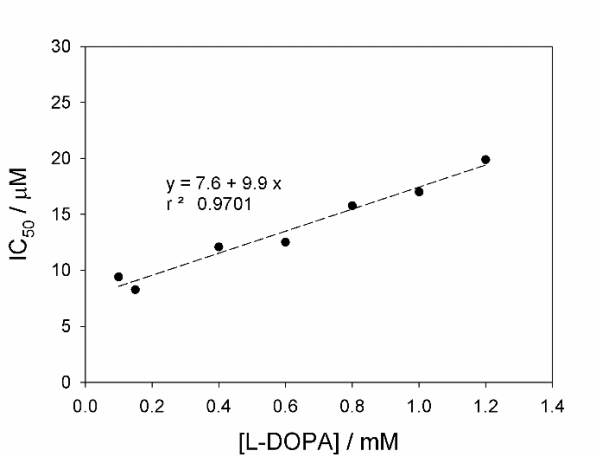

Figure S10. Plot of IC_{50} *vs* the concentration of substrate (L-DOPA) for diphenolase inhibition of mushroom tyrosinase by Kojic acid at 30°C (data from Table S4).

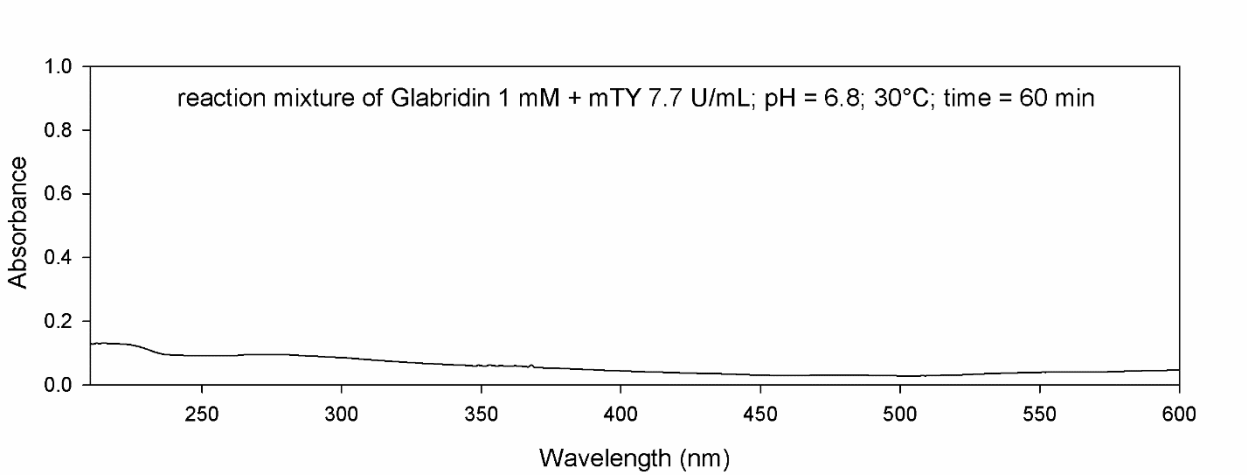

Figure S11. UV-Vis. difference spectrum obtained by subtracting from the spectrum of the reaction mixture composed by mushroom tyrosinase (7.7.U/mL) and 1 mM glabridin incubated at 30° for 1 hour (pH=6.8), the spectrum of glabridin at the same concentration in the same medium. No change or development of significant absorbtion suggests the absence of transformation of glabridin by the enzyme.

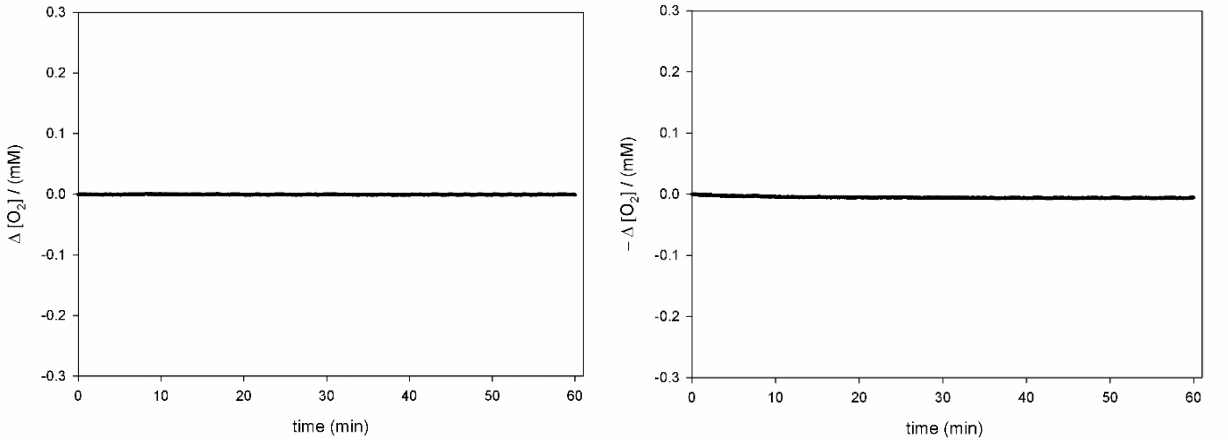

Figure S12. Oxygen consumption recorded by incubating mushroom tyrosinase (7.7.U/mL) with 200 nM glabridin (left panel) and 1 mM glabridin (right panel) at 30° for 1 hour (pH=6.8), in the absence of other substrates. No detectable oxygen consumption indicates no transformation of glabridin by the enzyme.